Structure-Based Design of Inhibitors with Improved Selectivity for Steroidogenic Cytochrome P450 17A1 over Cytochrome P450 21A2

Charlie Fehl,[†] Caleb D. Vogt,[‡] Rahul Yadav,[§] Kelin Li,[‡] Emily E. Scott,[*,§,∥] and Jeffrey Aubé[*,‡]

[†]Department of Medicinal Chemistry, University of Kansas, Lawrence, Kansas 66047, United States

[‡]Division of Chemical Biology and Medicinal Chemistry, UNC Eshelman School of Pharmacy, University of North Carolina at Chapel Hill, Chapel Hill, North Carolina 27599, United States

[§]Department of Medicinal Chemistry, University of Michigan, Ann Arbor, Michigan 48109, United States

[∥]Department of Pharmacology, University of Michigan, Ann Arbor, Michigan 48109, United States

ABSTRACT: Inhibition of androgen biosynthesis is clinically effective for treating androgen-responsive prostate cancer. Abiraterone is a clinical first-in-class inhibitor of cytochrome P450 17A1 (CYP17A1) required for androgen biosynthesis. However, abiraterone also causes hypertension, hypokalemia, and edema, likely due in part to off-target inhibition of another steroidogenic cytochrome P450, CYP21A2. Abiraterone analogs were designed based on structural evidence that B-ring substituents may favorably interact with polar residues in binding CYP17A1 and sterically clash with residues in the CYP21A2 active site. The best analogs increased selectivity of CYP17A1 inhibition up to 84-fold compared with 6.6-fold for abiraterone. Cocrystallization with CYP17A1 validated the intended new contacts with CYP17A1 active site residues. Docking these analogs into CYP21A2 identified steric clashes that likely underlie decreased binding and CYP21A2 inhibition. Overall, these analogs may offer a clinical advantage in the form of reduced side effects.

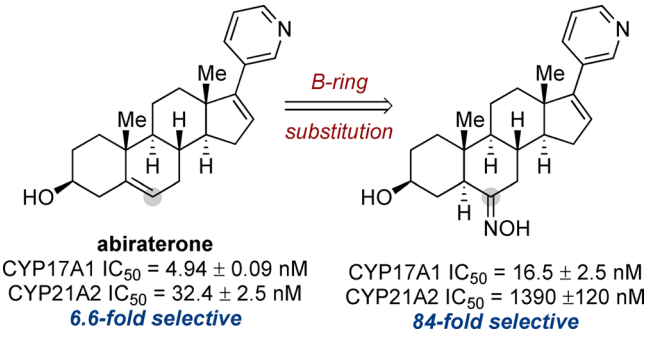

INTRODUCTION

In U.S. males, the cancer with the second highest death rate remains prostate cancer.[1] Prostate cancer proliferation is largely dependent on androgen signaling. Over 80% of tumors respond at least initially to surgical or chemical androgen deprivation therapy.[2] However, progression to the most aggressive form of this disease, castration-resistant prostate cancer, is frequently fatal despite best current therapeutic efforts. A recent addition to the drug arsenal for treatment of prostate cancer is abiraterone acetate, which extends overall survival for prostate cancer patients who had previously failed other treatment regimens.[3−5] Abiraterone acetate is a prodrug with abiraterone itself (Figure 1) being a tight-binding inhibitor of cytochrome P450 17A1 (CYP17A1). As CYP17A1 is the only human enzyme capable of converting C21 progestogens to the C19 androgens that frequently drive prostate cancer proliferation, this enzyme was an attractive target for systemic ablation of androgen biosynthesis (Figure 2A). Additionally, abiraterone is also currently being evaluated for hormone-responsive breast cancer, as estrogen synthesis is downstream of androgen synthesis. Other experimental therapeutics being developed in this class include the abiraterone analog galeterone[6,7] and nonsteroidal orteronel,[8] VT-464,[9] and BMS-351.[10]

Targeting CYP17A1 inhibition in this manner is efficacious clinically, but several serious side effects also became apparent early in clinical trials, including hypertension, hypokalemia, and edema.[11] Notably, many prostate cancer patients are older men for whom hypertension is frequently a preexisting concern. These side effects likely arise from abiraterone inhibiting not only just the CYP17A1 reactions but also inhibiting cytochrome P450 21A2 (CYP21A2) at clinically relevant concentrations.[12] Like CYP17A1, CYP21A2 hydroxylates progestogens such as progesterone and 17α-hydroxyprogesterone, but at C21 instead of C17 (Figure 2B). The resulting CYP21A2 products are intermediates in the production of the mineralocorticoid aldosterone and the glucocorticoid cortisol, thus impacting blood pressure control and potentially stress and immune responses. Crossover inhibition of CYP21A2 is not particularly surprising given that the two enzymes have the same fold, are 64% similar, bind some of the same substrates and/or products, and have a heme group for abiraterone pyridine coordination. Reducing abiraterone inhibition of CYP21A2 would likely reduce side effects without resorting to concomitant administration of the glucocorticoids prednisolone or dexamethasone, as is current clinical practice.[13]

Herein, structures of CYP17A1 and CYP21A2 were used to direct the design of abiraterone analogs with the goal of

Received: March 14, 2018
Published: May 24, 2018

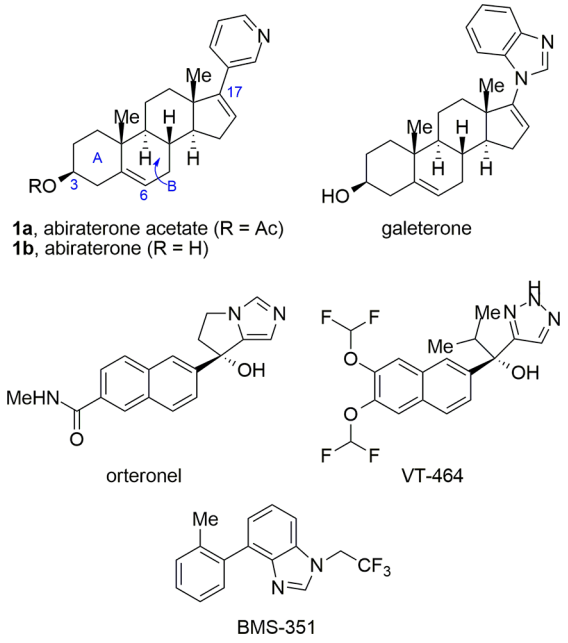

Figure 1. Structures of the marketed CYP17A1 inhibitor abiraterone acetate and related experimental therapeutics.

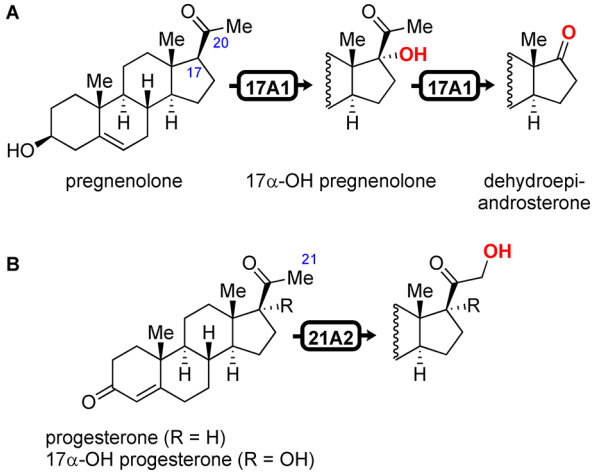

Figure 2. Key biosynthetic pathways involving (A) CYP17A1 and (B) CYP21A2 in human steroidogenesis. Progesterone is also a substrate for CYP17A1 17α-hydroxylation (not shown).

retaining effective CYP17A1 inhibition but decreasing CYP21A2 inhibition. Evaluation of these abiraterone analogs in steady-state inhibition studies with both enzymes revealed modifications increasing selectivity by more than 80-fold. By sparing CYP21A2 activity, these inhibitors could potentially allow more natural biosynthesis of mineralocorticoids and glucocorticoids to avoid severe hypertension, hyperkalemia, and edema, thereby reducing cardiovascular complications without compromising effective CYP17A1 inhibition in prostate cancer patients.

RESULTS AND DISCUSSION

Structure-Based Rationale for Inhibitor Design. Abiraterone is a structural analog of the CYP17A1 substrate pregnenolone (Figures 1 and 2A). CYP17A1 normally binds either pregnenolone or progesterone with C17 oriented toward the heme iron (Figure 3, yellow) for 17-hydroxylation (Figure 2A).[14] The resulting 17α-hydroxypregnenolone is then very subtly repositioned[14] for a second round of catalysis in the same active site to cleave the C17−C20 bond, resulting in the first androgen in the pathway, dehydroepiandrosterone (Figure 2A).[15] Both reactions require oxygen binding to the heme iron while adjacent to the substrate. The steroidal core of abiraterone (**1b**) is positioned similarly to these substrates, but contains a pyridine substituent projecting from C17 such that its heterocyclic nitrogen forms a coordinate-covalent bond with the heme iron, thereby occupying the position where oxygen would need to bind for catalysis to occur.[16]

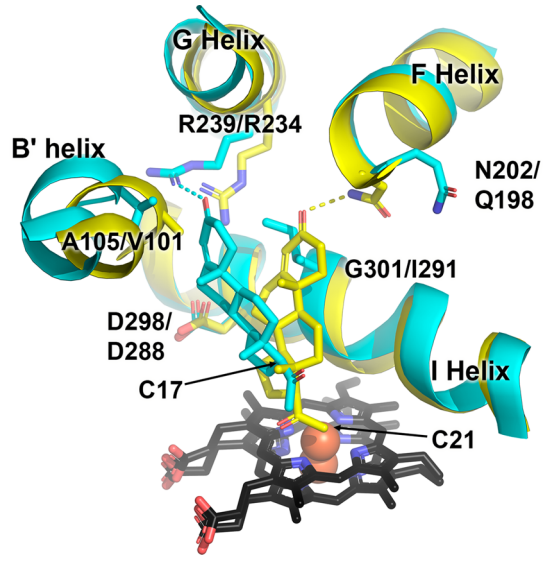

Figure 3. Comparison of human CYP17A1 (yellow) and CYP21A2 (cyan), both bound to progesterone (sticks). Orientation of the steroidal core is directed by (1) hydrogen bonding between the C3 oxygen and N202 in helix F for CYP17A1 vs R234 in helix G of CYP21A2, (2) a shift of the B′ helix outward and away from the active site in CYP21A2 compared to CYP17A1, and (3) substitution of I helix G301 in CYP17A1 for I291 in CYP21A2. Heme in black sticks with iron as central red sphere. Amino acids are labeled with the CYP17A1 residue given first, followed by the name of the CYP21A2 residue.

X-ray structures of human CYP17A1 with both abiraterone[16] and progesterone[14] reveal a similar binding mode for their steroidal cores. While a structure of human CYP21A2 has not been reported in complex with abiraterone, there is a structure of the CYP21A2/progesterone complex, and it is likely that the steroidal core of abiraterone would bind similarly to progesterone.[12] Comparison of these two steroidogenic enzymes each bound to progesterone align with a Cα root-mean-square deviation of only 1.9 Å, but reveal some informative differences to guide analog development. Despite conservation of the three polar residues lining the active site (N202/Q198, R239/R234, and D298/D288), progesterone is oriented differently in the two active sites, corresponding to the observed sites of metabolism. In CYP17A1, progesterone is oriented with C17 directed toward the heme, consistent with oxidation at this site. As a result, the steroidal core is oriented such that the C3 substituent on the opposite end forms a hydrogen bond with N202 in the F helix composing part of the active site roof (Figure 3, yellow). In CYP21A2, the long axis of the steroid core must adopt a different angle over the heme to position C21 for hydroxylation. Though N202 in CYP17A1 is conservatively substituted with Q198, the corresponding Q198

side chain in CYP21A2 is directed away from the active site, and in CYP21A2, the C3 substituent binds instead to R234 in the G helix, another major helix composing part of the active site roof (Figure 3, cyan). In addition, the B′ helix composing an adjacent wall of the active site is moved outward in CYP21A2 compared to its position in CYP17A1. In combination with substitution of G301 in CYP17A1 vs I291 in CYP21A2, such changes reapportion the active site volume available to ligands. With the goal of retaining CYP17A1 inhibition, the basic abiraterone scaffold was retained, with its N202- and heme-binding features. With the goal of reducing CYP21A2 inhibition, substituents or modifications of the B ring were employed. The hypothesis was that these modifications should occupy available space between R239 and D298 in the CYP17A1 active site and potentially engage in interactions with these two residues but be sterically less favorable in the CYP21A2 active site.

Chemistry. All compound syntheses stemmed from enol triflate **2**, a key intermediate in the large-scale production of abiraterone (**1b**; Scheme 1).[17] Thus, analog **3b**, which

Scheme 1. Synthesis of Abiraterone and Its Derivatives[a]

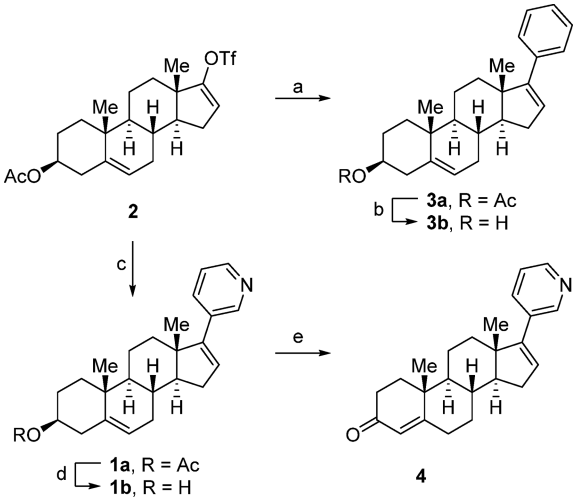

[a]Reagents and conditions: (a) phenylboronic acid, $Pd(PPh_3)_2Cl_2$, $NaHCO_3$, THF, H_2O, 60 °C, 23 h, 70%; (b) K_2CO_3, MeOH, rt, 16 h, 62%; (c) diethyl(3-pyridyl)borane, $Pd(PPh_3)_2Cl_2$, $NaHCO_3$, THF, H_2O, 60 °C, 23 h, 77%; (d) K_2CO_3, MeOH, rt, 17 h, 93%; (e) Al(O-*i*-Pr)$_3$, 2-butanone, toluene, reflux, 20 h, 60%.

substitutes the C17 pyridine ring for a phenyl, was prepared by modifying established procedures, namely, a Suzuki cross-coupling reaction followed by deprotection of the resulting acetate **3a**. Abiraterone itself provided the starting material for enone **4**, a key metabolite of the drug, using a previously reported[18,19] Oppenauer oxidation.

The first series of abiraterone analogs maintained the Δ^5-double bond found in the parent compound (Scheme 2). The enol triflate **2** provided a convenient starting point for diversification, as the Δ^5-double bond selectively reacted with *m*-CPBA to afford epoxide **5** in a ca. 2:1 mixture of the 5α,6α- and 5β,6β-diastereomers, respectively. Following cross-coupling, epoxide **6a** was obtained after recrystallization of a ca. 4:1 mixture from MeOH−H_2O (36% yield of pure **6a**). To reintroduce the Δ^5-double bond, an epoxide ring-opening was performed under basic conditions followed by elimination of the resulting tertiary alcohol. Depending on the choice of

Scheme 2. Analogs Prepared via Epoxidation of Enol Triflate 2[a]

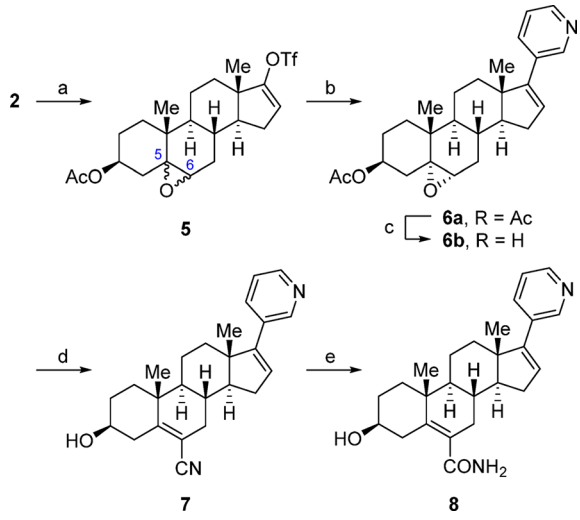

[a]Reagents and conditions: (a) *m*-CPBA, CH_2Cl_2, 0 °C to rt, 18 h, 90%; (b) diethyl(3-pyridyl)borane, $Pd(PPh_3)_2Cl_2$, $NaHCO_3$, THF, H_2O, 60 °C, 17 h, 36%; (c) K_2CO_3, MeOH, rt, 17 h, 99%; (d) KCN, MeOH, μW, 160 °C, 50 min, 63%; (e) NaOH, H_2O_2, MeOH, H_2O, rt, 46 h, 99%.

nucleophile, elimination could occur from the C4 or C6 carbon, potentially resulting in a mixture of Δ^4- and Δ^5-constitutionally isomers. In the case of epoxide-opening using cyanide, isomerization of the Δ^4-double bond (which would form from trans elimination of the β-oriented nitrile) should form the more conjugated Δ^5 olefin. Accordingly, epoxide **6a** was converted into nitrile **7** as a single isomer with potassium cyanide in methanol under microwave irradiation, effecting up to three transformations (including deprotection) in one step. Nitrile **7** was then hydrolyzed to amide **8** upon treatment with sodium hydroxide and hydrogen peroxide.

A series of saturated AB-ring analogs of 5α-abiraterone were also prepared (Scheme 3). Since *m*-CPBA reacted selectively at the Δ^5-double bond, it was likely that a hydroboration-oxidation reaction would also preferentially react at this position. Indeed, enol triflate **2**, when treated with 1.05 equiv of BH_3·THF, gave **9** in 28% yield along with 39% recovered starting material. The stereochemistry of **9** was assigned based on the coupling pattern of the C−6 methine (i.e., a triplet of doublets with a *J* value of 10.5 Hz for the triplet, suggesting two axial−axial couplings and therefore a β hydrogen atom) and confirmed by a strong NOE observed at the C-19 Me upon irradiation of the C-6 methine H (Supporting Information). The alcohol thus formed was converted to acetate **10a** after Suzuki cross-coupling and subsequently to diol **10b**. Alcohol **9** was also transformed into ketone **11** upon treatment with Dess−Martin periodinane, which was converted to ketone **12a** using the same sequence as **10b**. Ketones **12a** and **12b** were separately reacted with hydroxylamine hydrochloride to afford the corresponding oximes **13a** and **13b**. Finally, treatment of **13a** with thionyl chloride formed the ring expanded lactam **14a** via a Beckman rearrangement and **14b** following deacylation.

Inhibition of CYP17A1 and CYP21A2 *in Vitro* by Abiraterone and Its Analogs. These inhibitors were evaluated for their ability to differentially inhibit *in vitro* progesterone 17α-hydroxylation by CYP17A1 and progesterone 21-hydroxylation by CYP21A2. Initial experiments without

Scheme 3. Analogs Prepared via Hydroboration−Oxidation of Enol Triflate 2[a]

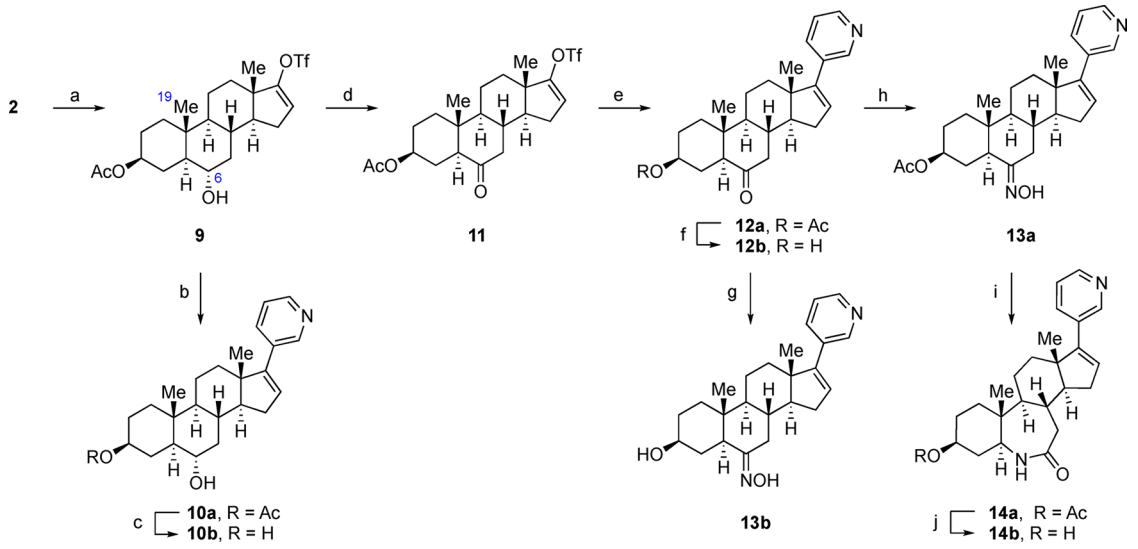

[a]Reagents and conditions: (a) BH_3·THF, THF, 0 °C, 4 h, then H_2O followed by $NaBO_3$·H_2O, 18 h, 0 °C to rt, 18 h, 28% (and 39% of recovered starting material); (b) diethyl(3-pyridyl)borane, $Pd(PPh_3)_2Cl_2$, $NaHCO_3$, THF, H_2O, 60 °C, 23 h, 49%; (c) K_2CO_3, MeOH, rt, 15 h, 97%; (d) Dess−Martin periodinane, CH_2Cl_2, 0 °C to rt, 16 h, 89%; (e) diethyl(3-pyridyl)borane, $Pd(PPh_3)_2Cl_2$, $NaHCO_3$, THF, H_2O, 60 °C, 17 h, 82%; (f) K_2CO_3, MeOH, rt, 17 h, 88%; (g) NH_2OH·HCl, NaOAc, EtOH, H_2O, rt, 17 h, 83%; (h) NH_2OH·HCl, NaOAc, EtOH, H_2O, rt, 24 h, 98%; (i) $SOCl_2$, THF, 0 °C, 4 h, then H_2O, 45%; (j) K_2CO_3, MeOH, rt, 17 h, 100%.

Table 1. IC_{50} Values for Inhibition of CYP17A1-Mediated Progesterone 17α-Hydroxylation and CYP21A2-Mediated Progesterone 21-Hydroxylation by Abiraterone and Its Analogs

entry	inhibitor	modification	CYP17A1 IC_{50} ± SE (nM)	CYP21A2 IC_{50} ± SE (nM)	CYP21A2 IC_{50}/CYP17A1 IC_{50}
1	abiraterone (**1b**)		4.94 ± 0.09	32.4 ± 2.5	6.6
2	galeterone		28.1 ± 2.3	77.2 ± 8.9	2.7
3	**3b**	17-phenyl	>20,000	≥700	
4	**4**	Δ^4, 4-oxo	6.13 ± 0.41	0.70 ± 0.03	0.11
5	**6b**	5α,6α-epoxide	7.83 ± 0.92	42.1 ± 8.5	5.4
6	**7**	Δ^4, C-6 CN	15.5 ± 2.7	23.9 ± 3.8	1.5
7	**8**	Δ^4, C-6 $CONH_2$	22.8 ± 1.5	673 ± 90	29
8	**10b**	5α-H, 6α-OH	7.2 ± 0.32	234 ± 32	33
9	**12b**	5α-H, 6-oxo	12.4 ± 0.49	440 ± 60	35
10	**13b**	5α-H, 6-oxime	16.5 ± 2.5	1390 ± 120	84
11	**14b**	B-ring expanded lactam	230 ± 51	3605 ± 1740	16

inhibitors with purified P450 enzymes and human NADPH-cytochrome P450 reductase were used to ensure that the progesterone substrate was not depleted and to evaluate the steady-state parameters. Progesterone 17α-hydroxylation by CYP17A1 resulted in a K_m of 6.8 ± 1.5 μM, similar to the previously reported value of 10.5 ± 1.7 μM.[14] Progesterone 21-hydroxylation by CYP21A2 occurred with a K_m of 0.37 ± 0.07 μM, also similar to the previously reported value of 0.21 ± 0.03 μM.[20] Thus, progesterone at 6 and 0.3 μM concentrations were used to determine the IC_{50} values for CYP17A1 and CYP21A2, respectively.

Abiraterone has been extensively studied as an inhibitor of CYP17A1, with reported IC_{50} values for progesterone 17α-hydroxylation ranging from 92 ± 4 to 9.4 ± 0.3 nM.[21] In the present study, an IC_{50} value of 4.94 ± 0.09 nM was determined for abiraterone inhibition of CYP17A1-mediated progesterone 17α-hydroxylation (Table 1). By comparison, abiraterone demonstrated an IC_{50} of 32.4 ± 2.5 nM for inhibition of CYP21A2-mediated progesterone 21-hydroxylation (Table 1). Thus, abiraterone itself is 6.6-fold more selective for CYP17A1 inhibition than CYP21A2 inhibition. The selectivity of galeterone (Figure 1), an abiraterone analog previously in clinical trials, was also evaluated and found to be less selective at 2.7-fold.

An initial abiraterone analog was constructed to quantitate the contribution of the pyridine nitrogen coordination to the heme iron. Interactions with nitrogen-containing heterocycles are known to contribute substantially to the affinity of inhibitors for cytochrome P450 enzymes but also contribute to nonselectivity across P450 enzymes, as is frequently observed for antifungal azoles. A notable example of this in the prostate cancer field was the early use of higher doses of the imidazole-containing antifugal ketoconazole as a treatment for prostate cancer due to its ability to inhibit CYP17A1 and thereby decrease systemic androgen production.[22] However, such usage frequently led to hepatotoxicity, potentially related to broad inhibition of hepatic drug-metabolizing enzymes, and is no longer recommended. Although contributions of this interaction to inhibitor affinity are well-known, the effects on inhibitor selectivity are not as clear.

Thus, analog **3b** was generated in which the C17 pyridine ring of abiraterone was substituted with a phenyl ring. As

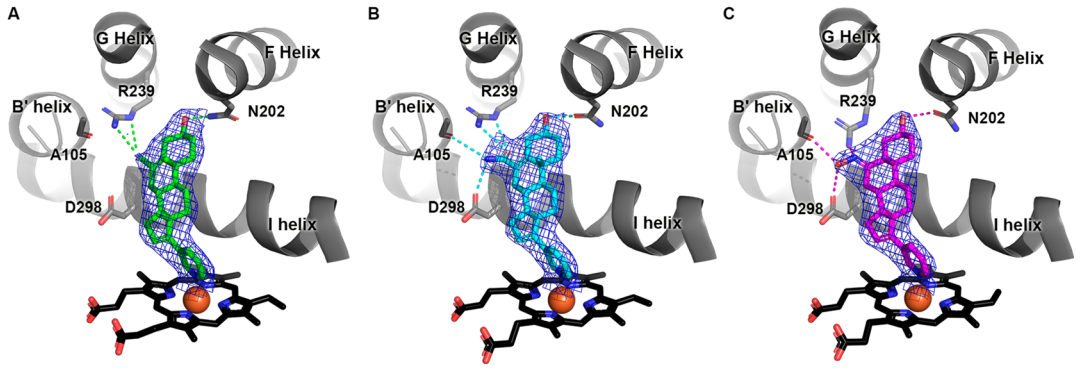

Figure 4. CYP17A1 X-ray structures with abiraterone analogs. Abiraterone analogs bearing (A) a C6 nitrile (**7**; green, 6CIZ), (B) a C6 amide (**8**; cyan, 6CHI), and (C) a C6 oxime (**13b**; magenta, 6CIR); key residues are shown as sticks. Interactions that fit the criteria for hydrogen bonding are indicated by dashed lines. Blue mesh represents the $|2F_o| - |F_c|$ electron density maps of the ligands contoured at 1.0σ. The heme is shown as black sticks with its iron as an orange sphere. Notably, the N202 side chain can be a hydrogen bond donor (A) or acceptor (B,C), as can the C3 hydroxyl.

anticipated, this compound demonstrated a substantial loss in affinity. The IC_{50} was increased more than 4000-fold to >20 μM for CYP17A1 and >20-fold to >0.7 μM for CYP21A2 (Table 1, entry 3). This compound is also more selective for inhibition of CYP21A2 rather than CYP17A1, opposite of the desired goal. Accordingly, all subsequent abiraterone analogs retained the pyridine.

Progesterone, which contains a Δ^4 double bond and a C3 ketone, differs in its interactions between the C3 ketone and different residues in the active site roof of CYP17A1 (N202 in the F helix) vs CYP21A2 (R234 in the G helix; see Figure 3 above). In addition, conversion of abiraterone to its Δ^4 metabolite leads to increased anticancer activity, in part due to greater androgen receptor antagonism.[19,23] This metabolite, compound **4**, has been reported to inhibit CYP17A1 comparably to abiraterone itself.[18] Similarly, little change was observed in the IC_{50} value of **4** against CYP17A1, but there was a 46-fold decrease in the IC_{50} for CYP21A2 (Table 1, entry 4). Thus, **4** was 8.8 times more selective for CYP21A2 over CY17A1 (Table 1), which was again opposite of the design goal. The IC_{50} curves for all analogs except **3b** are shown in Figure S1 (Supporting Information).

Analogs **7** and **8** retaining Δ^5 unsaturation and modifications at C6 were tested. These compounds largely maintained the ability to inhibit CYP17A1, with modest 3- and 4.6-fold increases in IC_{50} values for CYP17A1-mediated progesterone 17α-hydroxylation, respectively (Table 1, entries 6 and 7). However, the nitrile substitution in **7** did not significantly alter the IC_{50} for CYP21A2-mediated progesterone 21-hydroxylation, meaning that the **7** analog is less selective for CYP17A1 than abiraterone itself. In contrast, however, the C6 amide of **8** decreased inhibition of CYP21A2 by 20-fold to yield an IC_{50} > 600 nM. As a result, the selectivity increased from 6.6-fold for abiraterone itself to 29-fold with this modification, validating the idea that C6 substituents could play an important role in determining selectivity and suggesting that bulkier substitutions in this part of the molecule might be advantageous.

A second set of analogs lacking A/B unsaturation and containing modifications at C6 was examined. The epoxide **6b** behaved similarly to abiraterone in all respects (Table 1, entry 5). In contrast, analogs containing a C6α alcohol (**10b**) and C6 ketone (**12b**) resulted in markedly increased selectivity, mostly due to substantially poorer potency at CYP21A2 (entries 8 and 9). Even higher selectivity was observed for oxime **13b**. In this case, a ca. 3-fold increase in the IC_{50} for CYP17A1 was observed but was accompanied by a 43-fold increase in the IC_{50} for CYP21A2 (entry 10). Thus, this analog is ca. 84 times more selective for inhibition of CYP17A1 over CYP21A2 for their respective progesterone hydroxylation reactions.

An alternate strategy to incorporate ligand moieties that might engage with R239 and D298 in the CYP17A1 active site was to expand and modify the B ring. Thus, the B ring was replaced with a caprolactam ring (**14b**). This modification resulted in poorer potency against both targets (Table 1, entry 11), with ca. 16-fold selectivity for CYP17A1 over CYP21A2. Accordingly, no further analogs were pursued following this strategy.

X-ray Structures of Key CYP17A1/Inhibitor Complexes. In order to better understand interactions between CYP17A1 and some of the abiraterone inhibitor analogs tested herein, X-ray structures were determined with analogs incorporating the C6 nitrile **7**, the C6 amide **8**, and the C6 oxime **13b**. Complexes were formed by cocrystallization, and structures were determined (Supporting Information, Table S1) as described in the Experimental Section. The resulting structures revealed the same overall CYP17A1 conformation and placement of the steroidal core observed for other CYP17A1 steroidal substrates and inhibitors. All three abiraterone analogs retained (1) the interaction between the pyridine nitrogen and the heme iron and (2) a hydrogen bond between the C3 hydroxyl and N202 (Figure 4).

A 2.6 Å structure of CYP17A1 with the C6 nitrile (**7**) revealed that this substituent extended into the space between D298 and R239 as expected (Figure 4A). Its direct projection from the B ring displaced a water molecule often found in this position and places the nitrile N atom to accept hydrogen bonds from the side chain of R239 (2.9−3.5 Å for the two different interactions in the four different molecules CYP17A1/inhibitor complexes of the asymmetric unit). This occurred without significant reorientation of the R239 side chain compared to the abiraterone structure. No other significant changes were observed in the active site.

A 2.7 Å structure of CYP17A1 bound to the C6 amide analog (**8**) demonstrated the amide similarly positioned between the polar R239 and D298 side chains (Figure 4B). In this instance, the amide oxygen served as a hydrogen bond acceptor from the side chain of R239 (2.8−3.4 Å), whereas the amide nitrogen simultaneously formed a hydrogen bond donor to D298 (3.1−3.5 Å). Thus, this substituent engages both targeted polar residues in the CYP17A1 active site. In addition, the amide

nitrogen is placed to form a weak hydrogen bond (3.4−3.5 Å) with the backbone carbonyl of A105 in the B′ helix. Interestingly, the amide is twisted slightly out of conjugation with the Δ^5 olefin, suggesting some induced fit.

A 2.65 Å structure of CYP17A1 cocrystallized with the C6 oxime analog (**13b**) demonstrated that the oxime is projected somewhat similarly but above the plane between R239 and D298 (Figure 4C). As a result, the nitrogen is positioned to form a weak hydrogen bond (3.3−3.5 Å) with R239, while the substituent hydroxyl and D298 are similarly spaced for hydrogen bonding (3.2−3.3 Å). As in the case of the amide of **8**, the substituent hydroxyl of **13b** also engaged in an unanticipated hydrogen bond with the backbone carbonyl of A105 in the B′ helix, but in this case, the shorter distance suggests a stronger interaction (2.2−3.0 Å).

All three of these analogs were designed to specifically complement the CYP17A1 active site. Their IC_{50} values were only 1.2- to 4.6-fold higher than the parent abiraterone, and these structures revealed that they retained key interactions with the heme iron and N202, while the newly introduced B ring substituents were easily accommodated without changes in the CYP17A1 active site. Furthermore, the various substituents engaged in the intended new interactions with R239 in the G helix and D298 in the I helix, as well as making an unanticipated interaction with the backbone of the B′ helix. Since the B′ helix often has relatively few interactions with the rest of the P450 protein and has been implicated in conformational changes associated with ligand entry and exit, such interactions may lead to reduced inhibitor off rates.

Docking of Abiraterone Analogs into CYP17A1 and CYP21A2. While the structures above rationalized why several of these analogs bind and inhibit CYP17A1 similar to the parent abiraterone, the primary effects of such modifications were to increase selectivity by reducing inhibition of CYP21A2. As decreased CYP21A2 affinity is not likely to support cocrystallization of CYP21A2/inhibitor complexes, abiraterone and key compounds in this series (**7**, **6b**, **8**, **13b**, **12b**, **10b**) were docked into CYP17A1 and CYP21A2.

When abiraterone and each of these analogs were docked into CYP17A1, all analogs retained both (1) the hydrogen bond between C3 hydroxyl and the CYP17A1 N202 side chain and (2) pyridine nitrogen coordination to the heme iron, as exemplified in Figure 5. Compounds **7**, **8**, and **13b** docked into CYP17A1 reveal very similar conformations and hydrogen bonding to CYP17A1 residues as shown experimentally in the X-ray structures of CYP17A1 with these compounds. While the C6 substituents of **7** and **8** formed hydrogen bonds with either R239/D298 or both, the C6 substituent of **6b** did not make any contact with R239 and D298 upon docking. Similarly, the C6 hydroxyl substituent in **10b** and keto group of **12b** did not hydrogen bond with side chain D298 but did form weak hydrogen bonds with the side chain of R239. None of these docked compounds reveal significant unfavorable clashes with CYP17A1, and the favorable ΔG_{bind} ranges from −42 to −49 kcal/mol, consistent with relatively small differences between the IC_{50} values of these analogs for CYP17A1 (Table 2).

Progesterone docked into CYP21A2 very similarly to the X-ray structure shown in Figure 3, but docking abiraterone analogs into CYP21A2 revealed a number of key differences. Abiraterone itself docked in a similar orientation to progesterone, with the C3 OH hydrogen bonding to R234. However, docking of **8** into CYP21A2 revealed that R234 and D288 were involved in hydrogen bonding to the C6 amide

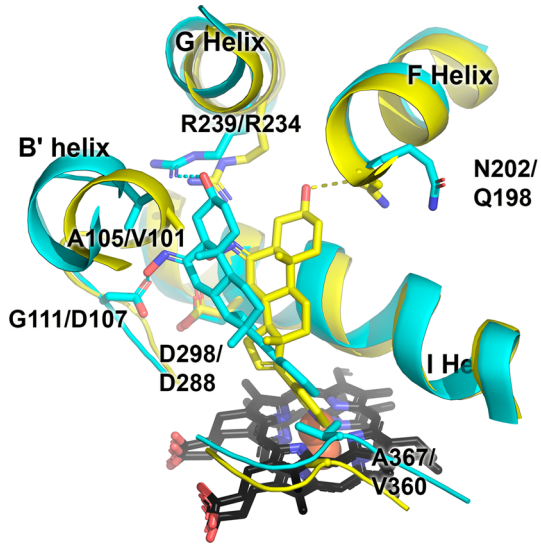

Figure 5. Compound **13b** (sticks) docked into human CYP17A1 (yellow; from PDB 3RUK, with bound abiraterone) and CYP21A2 (cyan; from PDB 4Y8W, with bound progesterone). Heme in black sticks with iron as central red sphere. While **13b** is accommodated in CYP17A similarly to abiraterone itself, in CYP21A2·**13b**, the only pose that could be docked at all has unfavorable interactions with D107 and V360. Amino acids are labeled with the CYP17A1 residue given first, followed by the name of the CYP21A2 residue.

Table 2. Statistics for Docking Abiraterone and Its Analogs into CYP17A1 and CYP21A2

	ΔG_{bind} (kcal/mol)	
inhibitor	CYP17A1	CYP21A2
abiraterone (**1b**)	−42.6	−11.9
8	−43.8	11.4
7	−42.6	−1.1
6b	−46.6	−6.4
12b	−48.0	2.4
10b	−46.6	−4.3
13b	−49.0	8.5

carbonyl and nitrogen, respectively. In this orientation, docked **8** resulted in unfavorable van der Waals energy for adjacent residues V287 and V360. Overall, the computed ΔG_{bind} was a highly unfavorable 11.4 kcal/mol for **8**, in comparison to −11.9 kcal/mol for abiraterone docked into CYP21A2. All conformers of compound **13b** failed to dock in the CYP21A2 except one. This single conformer (Figure 5) demonstrated a hydrogen bond between the C3 hydroxyl of **13b** and the side chain of R234, but no hydrogen bond between the C6 oxime and either R234 or D288. Instead, the oxime hydrogen bonded with the side chain of D107, but this side chain also imparts a large unfavorable van der Waals energy. As a result, the overall calculated ΔG_{bind} was also highly unfavorable at 8.5 kcal/mol. Docking **12b** into CYP21A2 suggested a hydrogen bond between its C3 hydroxyl and the side chain of R234 with no interaction with D288. Both the side chains of D107 and V360 resulted in unfavorable van der Waals interactions. Finally, docking of compounds **7**, **6b**, and **10b** into CYP21A2 suggested hydrogen bonds between the C3 hydroxyl and the R234 side chain. Again, a large unfavorable van der Waals interaction with V360 is calculated for **10b**, which is somewhat reduced for **7** and **6b**. The unfavorable van der Waals energy contribution

from V360 in CYP21A2 observed for many of the C6 substituted compounds appears to be ameliorated in CYP17A1 as this position is substituted by A367. Similarly, D107 in CYP21A2 is G111 in CYP17A1, which may also support binding to CYP17A1.

CONCLUSIONS

Using structure-based design, abiraterone analogs were generated that had IC_{50} values similar to the parent inhibitor for the target enzyme CYP17A1, but increased IC_{50} values for the off-target CYP21A2 enzyme by ca. 43-fold. This increased the 6.6-fold selectivity of abiraterone for CYP17A1 over CYP21A2 to as high as 84-fold, which was observed for the C6 oxime **13b**. The design strategy was to maintain CYP17A1 potency by adding substituents to the C6 of the steroid backbone able to engage in attractive hydrogen bonding interactions with the target but cause steric clashes with the off-target CYP21A2. These features were confirmed by X-ray crystallographic studies of three CYP17A1−inhibitor complexes and consistent with docking studies of the analogs with CYP21A2.

Although experimental testing with the full panel of human cytochrome P450 enzymes is beyond the scope of this article, we have briefly examined the behavior of compound **13b** vs abiraterone with respect to two key drug-metabolizing P450 enzymes. It is known that abiraterone is a substrate of CYP3A4 (formation of the *N*-oxide) and an inhibitor of the CYP2D6.[24] As a result, coadministration of CYP2D6 substrates with a narrow therapeutic index is not recommended for abiraterone. Accordingly, we tested CYP2D6 for inhibition by abiraterone against oxime **13b**. While the IC_{50} for abiraterone was 0.23 μM, the IC_{50} for **13b** was 8.57 μM, indicating that the potential for inhibition of CYP2D6 is actually decreased by 37-fold. Moreover, if abiraterone or its analogs are substrates for CYP3A4, then they ought to competitively inhibit substrate metabolism. However, our results show no significant inhibition of CYP3A4 by either abiraterone or **13b** up to concentrations of 640 nM. Since the C_{max} for abiraterone in patients is 90 nM under the typical dosing regimen, we do not anticipate this would be clinically significant.

Overall, reducing the off-target inhibition of CYP21A2 is expected to reduce the undesirable clinical side effects resulting from disruption of glucocorticoid and mineralocorticoid biosynthesis.

EXPERIMENTAL SECTION

General Information. All chemicals and solvents were purchased from commercial sources (Alfa Aesar, Ark Pharm, Oakwood Chemical, or Sigma-Aldrich) and used as received. Unless stated otherwise, reactions were performed under ambient conditions and monitored by thin-layer chromatography (TLC) using Analtech silica gel GHLF (250 μm) coated glass plates, which were visualized by either shortwave UV light or cerium ammonium molybdate (CAM) stain. Normal or reverse phase chromatography was carried out on a Teledyne Isco Combiflash purification system. Microwave reactions were performed using a Biotage Initiator Classic with an autosampler. All nuclear magnetic resonance (NMR) spectra (^{1}H, ^{13}C, and ^{19}F) were recorded in deuterated solvents ($CDCl_3$ or DMSO-d_6) on a Varian 400 MR NMR spectrometer. Chemical shifts are reported in parts per million (ppm) and were adjusted using the residual undeuterated solvents ($CDCl_3$: 7.26 ppm for ^{1}H NMR, 77.2 ppm for ^{13}C NMR; DMSO-d_6: 2.50 ppm for ^{1}H NMR, 39.5 ppm for ^{13}C NMR) as an internal reference. Using the unified scale, ^{19}F NMR spectra were referenced with respect to the ^{1}H frequency of tetramethylsilane (TMS).[25] Coupling constants are reported in Hertz (Hz), and peak multiplicities as either a singlet (s), doublet (d), triplet (t), multiplet (m), or complex. Infrared (IR) spectra were acquired on a Thermo Scientific Nicolet iS 50 FT-IR Spectrometer. Melting points were determined on an Optimelt MPA100 instrument and are uncorrected. Optical rotations were measured with a Rudolph AUTOPOL IV. High-resolution mass spectrometry (HRMS) data were collected on a Thermo Electron hybrid ion trap FT-ICR mass spectrometer equipped with a 7T ICR magnet (LTQ-FT) using either an electrospray ionization (ESI) or atmospheric-pressure chemical ionization (APCI) source. Purity data were measured with a Waters ACQUITY UPLC H-Class System coupled to the aforementioned mass spectrometer with the ESI source. All samples were prepared in MeOH at a concentration of 1 mg/mL, and 3 μL of each solution was introduced at a flow rate of 0.6 mL/min onto a Waters Acquity UPLC BEH C18 column (2.1 × 50 mm, 1.7 um particle size) at 40 °C. The solvent gradient was as follows: H_2O with 0.1% formic acid ramped linearly over 9.80 min to 95% MeCN with 0.1% formic acid and held for 0.40 min. At 10.21 min, the gradient was switched back to H_2O and allowed to re-equilibrate for 1.05 min to prepare for the next sample. Compound purity was determined on the basis of peak integration (area under the curve) from the total ion chromatogram (TIC), and HRMS data provided verification of compound identity. All compounds used for biological studies had an LC purity of >95%.

General Procedure A for Suzuki Cross-Coupling. A flame-dried flask was charged with the appropriate enol triflate, either 3-(diethylboranyl) pyridine or phenylboronic acid, and bis-(triphenylphosphine)palladium(II) dichloride. After vacuum flushing with Ar (×3), anhydrous THF was added, followed by a saturated solution of $NaHCO_3$ that had been sparged with N_2 for 15 min prior to addition. The reaction mixture was heated to 60 °C and stirred overnight. After cooling to rt, the solvent was removed under a stream of N_2. The resulting black residue was dissolved in CH_2Cl_2 and washed with H_2O, and the aqueous layer were extracted with CH_2Cl_2 (×2). The combined organic layers were dried over $MgSO_4$, filtered, and concentrated. The crude product was purified by chromatography to afford the corresponding pyridyl or phenyl compound.

General Procedure B for Acetate Deprotection. A vial was charged with the appropriate acetate, K_2CO_3, and MeOH. After stirring overnight, the reaction was quenched with a saturated solution of NH_4Cl, and the aqueous layer was extracted with CH_2Cl_2 (×3). The combined organic layers were dried over $MgSO_4$, filtered, and concentrated. The crude product was purified by chromatography to afford the corresponding alcohol.

General Procedure C for Oxime Formation. A vial was charged with the appropriate ketone, NH_2OH·HCl, NaOAc, EtOH, and H_2O. The reaction mixture was stirred vigorously overnight and then concentrated under a stream on N_2. The white solid was dissolved in CH_2Cl_2. The organic layer was washed with H_2O, and the aqueous layer was extracted with CH_2Cl_2. The combined organic layers were dried over Na_2SO_4, filtered, and concentrated. The crude product was purified by chromatography to afford the corresponding oxime.

*17-(3-Pyridyl)androsta-5,16-dien-3β-yl Acetate (Abiraterone Acetate, **1a**).*[17,26] Following general procedure A, **2** (0.501 g, 1.08 mmol) was coupled to 3-(diethylboranyl) pyridine (0.181 g, 1.23 mmol, 1.1 equiv) using bis(triphenylphosphine)palladium(II) dichloride (77.5 mg, 110 μmol, 0.1 equiv) in anhydrous THF (6.5 mL) and a saturated solution of $NaHCO_3$ (2.2 mL) for 23 h. After workup, the crude product was purified by chromatography (12 g of silica gel, 0−50% EtOAc/hexanes) to afford **1a** (0.326 g, 0.833 mmol, 77% yield) as a white, amorphous solid. R_f = 0.6 (50% EtOAc in hexanes); ^{1}H NMR (400 MHz, $CDCl_3$) δ 8.61 (d, J = 2.1 Hz, 1H), 8.45 (dd, J = 4.9, 1.6 Hz, 1H), 7.64 (dt, J = 7.9, 1.7 Hz, 1H), 7.21 (dd, J = 7.9, 4.8 Hz, 1H), 5.99 (dd, J = 3.3, 1.8 Hz, 1H), 5.41 (d, J = 5.2 Hz, 1H), 4.68−4.55 (m, 1H), 2.41−2.29 (m, 2H), 2.26 (ddd, J = 15.8, 6.5, 3.3 Hz, 1H), 2.10−2.04 (m, 2H), 2.03 (s, 3H), 1.91−1.82 (m, 2H), 1.76−1.54 (complex, 7H), 1.53−1.43 (m, 2H), 1.20−1.10 (m, 1H), 1.08 (s, 3H), 1.04 (s, 3H); ^{13}C NMR (101 MHz, $CDCl_3$) δ 170.7, 151.8, 148.1, 148.0, 140.2, 133.8, 133.1, 129.3, 123.1, 122.4, 74.0, 57.6, 50.4, 47.5, 38.3, 37.1, 36.9, 35.4, 31.9, 31.6, 30.6, 27.9, 21.6, 21.0, 19.4, 16.7; IR (neat)

1732 cm^{-1}; mp 142−145 °C, lit.[17] 144−145 °C (hexanes); $[\alpha]_D^{21}$ −49.2 (*c* 1.00, $CHCl_3$); HRMS (ESI) *m/z* $[M + H]^+$ calcd for $C_{26}H_{34}NO_2$ 392.2584; found 392.2576.

17-(3-Pyridyl)androsta-5,16-dien-3β-ol (Abiraterone, ***1b****).*[17,26] Following general procedure B, **1a** (60.5 mg, 0.155 mmol) was reacted with K_2CO_3 (0.212 g, 1.53 mmol, 10.0 equiv) in MeOH (5.1 mL) for 17 h. After workup, the crude product was purified by chromatography (4 g of silica gel, 0−60% EtOAc/hexanes) to afford **1b** (50.3 mg, 93% yield) as a white, amorphous solid. R_f = 0.5 (60% EtOAc/hexanes); ^{1}H NMR (400 MHz, $CDCl_3$) δ 8.62 (d, *J* = 2.1 Hz, 1H), 8.45 (dd, *J* = 4.8, 1.5 Hz, 1H), 7.64 (dt, *J* = 7.9, 2.0 Hz, 1H), 7.21 (dd, *J* = 7.9, 4.8 Hz, 1H), 5.99 (dd, *J* = 3.4, 1.8 Hz, 1H), 5.41−5.37 (m, 1H), 3.59−3.49 (m, 1H), 2.36−2.20 (m, 3H), 2.12−2.00 (m, 3H), 1.89−1.81 (m, 2H), 1.80−1.43 (complex, 8H), 1.15−1.10 (m, 2H), 1.07 (s, 3H), 1.05 (s, 3H); ^{13}C NMR (101 MHz, $CDCl_3$) δ 151.8, 148.1, 148.0, 141.3, 133.8, 133.1, 129.4, 123.2, 121.5, 71.8, 57.7, 50.5, 47.5, 42.5, 37.3, 36.9, 35.4, 32.0, 31.8, 31.7, 30.6, 21.0, 19.5, 16.7; IR (neat) 3221, 1446 cm^{-1}; mp 224−227 °C, lit.[17] 228−229 °C (toluene); $[\alpha]_D^{22}$ −63.4 (*c* 1.00, $CHCl_3$); HRMS (ESI) *m/z* $[M + H]^+$ calcd for $C_{24}H_{32}NO$ 350.2478; found 350.2470; LCMS t_R = 4.86 min.

*3β-Acetoxyandrosta-5,16-dien-17-yl Trifluoromethanesulfonate (****2****).*[17,27] A flame-dried 250 mL round-bottom flask was charged with **15** (16.0 g, 48.4 mmol), 2,6-lutidine (11.3 mL, 97.0 mmol, 2.0 equiv), and anhydrous CH_2Cl_2 (320 mL) under Ar. The reaction mixture was cooled to −78 °C, and Tf_2O (15 mL, 87 mmol, 1.8 equiv) was added dropwise over 30 min. The reaction mixture was stirred at −78 °C for 2 h and then stored in a −20 °C freezer for 16 h. While the reaction mixture was still cold, a solution of 1 N HCl (200 mL) was added, and the aqueous layer was extracted with CH_2Cl_2 (200 mL). The combined organic layers were washed with brine (200 mL), dried over Na_2SO_4, filtered, and concentrated. The crude product was purified by chromatography (500 g of silica gel, 25% EtOAc/hexanes) to afford **2** (17.0 g, 36.7 mmol, 76% yield) as an off-white, amorphous solid. An analytical sample was prepared by recrystallization from MeOH−H_2O. R_f = 0.4 (10% EtOAc in hexanes); ^{1}H NMR (400 MHz, $CDCl_3$) δ 5.58 (dd, *J* = 3.3, 1.6 Hz, 1H), 5.39 (d, *J* = 5.3 Hz, 1H), 4.67−4.53 (m, 1H), 2.39−2.28 (m, 2H), 2.23 (ddd, *J* = 14.9, 6.2, 3.4 Hz, 1H), 2.03 (s, 3H), 2.01−1.94 (m, 1H), 1.92−1.81 (m, 2H), 1.80−1.74 (m, 1H), 1.72−1.52 (m, 6H), 1.52−1.42 (m, 2H), 1.21−1.05 (m, 2H), 1.05 (s, 3H), 0.99 (s, 3H); ^{13}C NMR (101 MHz, $CDCl_3$) δ 170.6, 159.3, 140.3, 121.9, 118.7 (q, *J* = 321 Hz), 114.6, 73.8, 54.4, 50.5, 44.8, 38.2, 37.0, 36.9, 32.8, 30.7, 30.1, 28.7, 27.8, 21.6, 20.3, 19.3, 15.2; ^{19}F NMR (376 MHz, $CDCl_3$) δ −73.6 (s); IR (thin film) 1732, 1629 cm^{-1}; mp 73−76 °C (MeOH−H_2O), lit.[17] 75−76 °C (hexanes); $[\alpha]_D^{23}$ −51.8 (*c* 1.00, $CHCl_3$); HRMS (APCI) *m/z* $[M - CH_3CO_2]^+$ calcd for $C_{20}H_{36}F_3O_3S$ 403.1549; found 403.1543.

*17-Phenylandrosta-5,16-dien-3β-yl Acetate (****3a****).* Following general procedure A, **2** (0.199 g, 0.430 mmol) was coupled to phenylboronic acid (60.5 mg, 0.496 mmol, 1.1 equiv) using bis(triphenylphosphine)palladium(II) dichloride (31.1 mg, 44.0 μmol, 0.1 equiv) in anhydrous THF (2.9 mL) and a saturated solution of $NaHCO_3$ (0.86 mL) for 23 h. After workup, the crude product was purified by chromatography (12 g of silica gel, 0−5% EtOAc/hexanes) to afford **3a** (0.117 g, 0.301 mmol, 70% yield) as a white, amorphous solid. R_f = 0.6 (10% EtOAc/hexanes); ^{1}H NMR (400 MHz, $CDCl_3$) δ 7.39−7.35 (m, 2H), 7.32−7.27 (m, 2H), 7.25−7.20 (m, 1H), 5.91 (dd, *J* = 3.4, 1.8 Hz, 1H), 5.45−5.39 (m, 1H), 4.67−4.56 (m, 1H), 2.39−2.29 (m, 2H), 2.23 (ddd, *J* = 15.6, 6.5, 3.3 Hz, 1H), 2.13−1.98 (m, 3H), 2.04 (s, 3H), 1.92−1.83 (m, 2H), 1.81−1.73 (complex, 8H), 1.21−1.10 (m, 1H), 1.09 (s, 3H), 1.06 (s, 3H); ^{13}C NMR (101 MHz, $CDCl_3$) δ 170.7, 154.9, 140.2, 137.5, 128.2 (2C), 127.3, 126.8 (3C), 122.6, 74.1, 57.7, 50.5, 47.7, 38.3, 37.1, 37.0, 35.5, 31.8, 31.7, 30.6, 27.9, 21.6, 21.0, 19.4, 16.8; IR (neat) 1731 cm^{-1}; mp 141−144 °C; $[\alpha]_D^{22}$ −58.0 (*c* 1.00, $CHCl_3$); HRMS (APCI) *m/z* $[M - CH_3CO_2]^+$ calcd for $C_{25}H_{31}$ 331.2420; found 331.2415.

*17-Phenylandrosta-5,16-dien-3β-ol (****3b****).* Following general procedure B, **3a** (78.1 mg, 0.200 mmol) was reacted with K_2CO_3 (0.275 g, 1.99 mmol, 10.0 equiv) in MeOH (6.7 mL) for 16 h. After workup, the crude product was purified by chromatography (4 g of silica gel, 0−25% EtOAc/hexanes) to afford **3b** (43.2 mg, 0.124 mmol, 62% yield) as a white, amorphous solid. R_f = 0.4 (25% EtOAc/hexanes); ^{1}H NMR (400 MHz, $CDCl_3$) δ 7.40−7.36 (m, 2H), 7.33−7.27 (m, 2H), 7.25−7.20 (m, 1H), 5.92 (dd, *J* = 3.3, 1.8 Hz, 1H), 5.42−5.38 (m, 1H), 3.60−3.49 (m, 1H), 2.37−2.19 (m, 3H), 2.14−1.99 (m, 3H), 1.90−1.81 (m, 2H), 1.81−1.44 (complex, 8H), 1.15−1.02 (m, 2H), 1.08 (s, 3H), 1.07 (s, 3H); ^{13}C NMR (101 MHz, $CDCl_3$) δ 154.9, 141.2, 137.5, 128.2 (2C), 127.3, 126.8 (3C), 121.6, 71.9, 57.8, 50.6, 47.3, 42.5, 37.3, 36.8, 35.5, 31.79, 31.76, 31.7, 30.6, 21.1, 19.5, 16.8; IR (neat) 3258 cm^{-1}; mp 150−154 °C; $[\alpha]_D^{22}$ −70.1 (*c* 1.00, $CHCl_3$); HRMS (APCI) *m/z* $[M - OH]^+$ calcd for $C_{25}H_{31}$ 331.2420; found 331.2420; LCMS t_R = 8.95 min.

*17-(3-Pyridyl)androsta-4,16-dien-3-one (****4****).*[17,18] Prepared by adapting a previously reported procedure. A flame-dried 25 mL round-bottom flask was charged with **1b** (0.250 g, 0.715 mmol), butan-2-one (2.2 mL, 25 mmol, 35 equiv), and anhydrous toluene (7.3 mL) under Ar. The reaction mixture was heated to reflux for 20 h. After cooling to rt, the reaction mixture was concentrated and diluted with EtOAc (30 mL). The organic layer was washed with brine (20 mL), and the aqueous layer was extracted with EtOAc (30 mL). The combined organic layers were dried over Na_2SO_4, filtered, and concentrated. The crude product was purified by chromatography (12 g of silica gel, 0−50% EtOAc/hexanes) to afford **4** as a white, amorphous solid (0.150 g, 0.430 mmol, 60% yield). An analytical sample was prepared through recrystallization from MeOH−H_2O. R_f = 0.3 (50% EtOAc/hexanes); ^{1}H NMR (400 MHz, $CDCl_3$) δ 8.61 (d, *J* = 2.3 Hz, 1H), 8.46 (dd, *J* = 4.7, 1.3 Hz, 1H), 7.63 (dt, *J* = 7.9, 1.8 Hz, 1H), 7.21 (dd, *J* = 7.6, 4.8 Hz, 1H), 5.98 (dd, J = 3.3, 1.8 Hz, 1H), 5.75 (s, 1H), 2.53−2.22 (complex, 5H), 2.15−1.98 (m, 3H), 1.97−1.87 (m, 1H), 1.86−1.77 (m, 1H), 1.76−1.64 (m, 2H), 1.63−1.42 (m, 3H), 1.23 (s, 3H), 1.22−0.99 (m, 2H), 1.06 (s, 3H); ^{13}C NMR (101 MHz, $CDCl_3$) δ 199.5, 171.0, 151.7, 148.2, 148.0, 133.8, 132.9, 129.2, 124.2, 123.2, 56.9, 54.1, 47.4, 38.8, 35.7, 35.2, 34.3, 34.1, 32.9, 31.9, 31.8, 21.0, 17.4, 16.8; IR (neat) 1665, 1610 cm^{-1}; mp 145−147 °C (MeOH−H_2O), lit.[17] 148−150 °C (Et_2O); $[\alpha]_D^{22}$ +138 (*c* 1.00, $CHCl_3$); HRMS (ESI) *m/z* $[M + H]^+$ calcd for $C_{24}H_{30}NO$ 348.2322; found 348.2316; LCMS t_R = 4.79 min.

*3β-Acetoxy-5α,6α-epoxyandrost-16-en-17-yl Trifluoromethanesulfonate (****5α,6α-5****) and 3β-Acetoxy-5β,6β-epoxyandrost-16-en-17-yl Trifluoromethanesulfonate (****5β,6β-5****).* A 100 mL round-bottom flask was charged with **2** (1.60 g, 3.46 mmol) and anhydrous CH_2Cl_2 (35 mL). The reaction mixture was cooled to 0 °C, and *m*-CPBA (77 wt %, 0.775 g, 3.46 mmol, 1.0 equiv) was added in one portion. The reaction mixture was allowed to warm to rt and stirred for 18 h. Afterward, the reaction mixture was diluted with CH_2Cl_2 (100 mL) and washed with a saturated solution of $NaHCO_3$ (100 mL). The aqueous layer was extracted with CH_2Cl_2 (50 mL). The combined organic layers were dried over $MgSO_4$, filtered, and concentrated. The crude product was purified by chromatography (40 g of silica gel, 0−10% EtOAc/hexanes) to afford an inseparable mixture of **5α,6α-5** and **5β,6β-5** (1.49 g, 3.12 mmol, 90% yield) in a ca. 2:1 ratio (determined by ^{1}H NMR) as a clear, colorless oil, which solidified into a white, amorphous solid upon standing. R_f = 0.1 (10% EtOAc/hexanes); **5α,6α-5** (major diastereomer): ^{1}H NMR (400 MHz, $CDCl_3$) δ 5.59−5.42 (m, 1H), 5.01−4.88 (m, 1H), 2.91 (dd, *J* = 4.5, 1.3 Hz, 1H), 2.26−1.89 (complex, 5H), 2.00 (d, *J* = 1.4 Hz, 3H), 1.76−1.22 (complex, 12H), 1.10 (s, 3H), 0.92 (s, 3H); ^{13}C NMR (101 MHz, $CDCl_3$) δ 170.3, 159.1, 118.7 (q, *J* = 321 Hz), 114.3, 71.3, 65.4, 58.7, 54.2, 44.8, 42.8, 36.2, 35.4, 32.4, 32.1, 28.5, 28.1, 27.5, 27.3, 21.5, 20.0, 16.0, 15.16; ^{19}F NMR (376 Hz, $CDCl_3$) δ −73.60 (s). **5β,6β-5** (minor diastereomer, diagnostic peaks only): ^{1}H NMR (400 MHz, $CDCl_3$) δ 4.82−4.68 (m, 1H), 3.13−3.10 (m, 1H), 2.02 (d, *J* = 1.5 Hz, 3H), 1.88−1.79 (m, 1H), 1.03 (s, 3H), 0.94 (s, 3H); ^{13}C NMR (101 MHz, $CDCl_3$) δ 170.7, 159.2, 114.3, 71.2, 63.3, 62.8, 54.0, 51.6, 44.7, 38.1, 36.8, 35.5, 32.8, 31.5, 28.7, 28.0, 21.4, 21.0, 17.1, 15.24; ^{19}F NMR (376 Hz, $CDCl_3$) δ −73.61 (s). **5α,6α-5** and **5β,6β-5**: IR (thin film) 1732, 1628 cm^{-1}; HRMS (APCI) *m/z* $[M - CH_3CO_2]^+$ calcd for $C_{20}H_{26}F_3O_4S$ 419.1498; found 419.1497.

*5α,6α-Epoxy-17-(3-pyridyl)androst-16-en-3β-yl acetate (****6a****) and 5β,6β-Epoxy-17-(3-pyridyl)androst-16-en-3β-yl acetate (****5β,6β-6a****).* Following general procedure A, **5** (3.00 g, 6.27 mmol) was coupled to

3-(diethylboranyl)pyridine (1.04 g, 7.10 mmol, 1.1 equiv) using bis(triphenylphosphine)palladium(II) dichloride (0.440 g, 0.627 mmol, 0.1 equiv) in anhydrous THF (37 mL) and a saturated solution of $NaHCO_3$ (12.5 mL) for 17 h. After workup, the crude product was purified by chromatography (80 g of silica gel, 0−50% EtOAc/hexanes) to afford a mixture of **6a** and **5β,6β-6a** (1.65 g, 4.06 mmol, 65% yield) in a ca. 4:1 ratio (determined by ^{1}H NMR) as an off-white, amorphous solid. Some of this material (0.572 g, 1.40 mmol) was recrystallized from MeOH−H_2O to give an analytical sample of **6a** (0.208 g, 0.511 mmol, 36% recovery) as a white, crystalline solid. R_f = 0.3 (50% EtOAc/hexanes); **6a** (major diastereomer): ^{1}H NMR (400 MHz, $CDCl_3$) δ 8.58 (s, 1H), 8.44 (d, J = 3.9 Hz, 1H), 7.60 (dt, J = 8.0, 2.0 Hz, 1H), 7.19 (dd, J = 8.0, 4.8 Hz, 1H), 5.97−5.93 (m, 1H), 5.01−4.89 (m, 1H), 2.94 (d, J = 4.5 Hz, 1H), 2.31−2.11 (m, 2H), 2.07−1.93 (complex, 4H), 2.02 (s, 3H), 1.90−1.31 (complex, 12H), 1.13 (s, 3H), 0.96 (s, 3H); ^{13}C NMR (101 MHz, $CDCl_3$) δ 170.3, 151.7, 148.1, 148.0, 133.8, 132.9, 129.1, 123.1, 71.4, 65.5, 59.0, 57.4, 47.4, 42.6, 36.2, 35.4, 35.0, 32.1, 31.7, 28.6, 28.5, 27.3, 21.5, 20.6, 16.6, 16.0; IR (neat) 1732 cm^{-1}; mp 197−200 °C (MeOH−H_2O); $[\alpha]_D^{22}$ −52.7 (c 1.00, $CHCl_3$); HRMS (ESI) m/z [M + H]$^+$ calcd for $C_{26}H_{34}NO_3$ 408.2533; found 408.2547. **5β,6β-6a** (minor diastereomer, diagnostic peaks only): ^{1}H NMR (400 MHz, $CDCl_3$) δ 4.82−4.73 (m, 1H), 3.13 (d, J = 2.6 Hz, 1H), 2.03 (s, 3H), 1.05 (s, 3H), 1.00 (s, 3H); ^{13}C NMR (101 MHz, $CDCl_3$) δ 170.7, 151.7, 150.0, 149.3, 136.7, 133.8, 63.6, 63.5, 62.8, 57.2, 51.5, 51.4, 47.4, 45.3, 38.1, 36.8, 35.4, 32.4, 31.9, 21.7, 17.2, 16.7.

*5α,6α-Epoxy-17-(3-pyridyl)androst-16-en-3β-ol (**6b**).* Following general procedure B, **6a** (49.8 mg, 0.122 mmol) was reacted with K_2CO_3 (0.170 g, 1.23 mmol, 10.1 equiv) in MeOH (4.2 mL) for 17 h. After workup, the crude product was purified by chromatography (4 g of silica gel, 0−5% MeOH/CH_2Cl_2) to afford **6b** (44.4 mg, 0.121 mmol, 99% yield) as a white, amorphous solid. R_f = 0.4 (5% MeOH/CH_2Cl_2); ^{1}H NMR (400 MHz, $CDCl_3$) δ 8.58 (dd, J = 2.3, 0.9 Hz, 1H), 8.44 (dd, J = 4.9, 1.6 Hz, 1H), 7.61 (dt, J = 7.9, 2.0 Hz, 1H), 7.20 (ddd, J = 7.9, 4.8, 0.9 Hz, 1H), 5.96 (dd, J = 3.3, 1.8 Hz, 1H), 3.97−3.87 (m, 1H), 2.95 (d, J = 4.5 Hz, 1H), 2.25 (ddd, J = 15.7, 6.5, 3.3 Hz, 1H), 2.10 (dd, J = 12.7, 11.4 Hz, 1H), 2.05−1.89 (complex, 4H), 1.73−1.58 (complex, 5H), 1.58−1.36 (complex, 6H), 1.36−1.29 (m, 1H), 1.12 (s, 3H), 0.97 (s, 3H); ^{13}C NMR (101 MHz, $CDCl_3$) δ 151.7, 148.0 (2C), 133.8, 133.0, 129.2, 123.1, 68.7, 66.0, 59.2, 57.5, 47.5, 42.8, 40.0, 35.2, 35.0, 32.4, 31.7, 31.2, 28.6, 28.5, 20.7, 16.6, 16.1; IR (neat) 3389, 3180 cm^{-1}; mp 239−242 °C; $[\alpha]_D^{21}$ −55.6 (c 1.00, $CHCl_3$); HRMS (ESI) m/z [M + H]$^+$ calcd for $C_{24}H_{32}NO_2$ 366.2428; found 366.2427; LCMS t_R = 3.81 min.

*3β-Hydroxy-17-(3-pyridyl)androsta-5,16-dien-6-carbonitrile (**7**).* A 10 mL microwave vial was charged with a ca. 4:1 mixture of **6a** and **5β,6β-6a** (0.251 g, 0.547 mmol), KCN (0.399 g, 6.13 mmol, 11.2 equiv), and MeOH (5.0 mL). **CAUTION:** KCN is highly toxic and must be handled with care! The reaction mixture was stirred at 160 °C for 50 min using a microwave reactor (time measured when the reaction mixture reached the programmed temperature after a ramp period of ca. 1 min). After cooling to rt, the reaction mixture was concentrated. The residue was dissolved in CH_2Cl_2 (25 mL) and washed with H_2O (50 mL). The aqueous layer was extracted with CH_2Cl_2 (2 × 25 mL), and the combined organic layers were concentrated. The crude product was purified by chromatography (150 g of C18 silica gel, H_2O containing 0.1 vol % NH_4OH/MeCN) to afford **7** (0.145 g, 0.388 mmol, 63% yield) as an off-white, amorphous solid. An analytical sample was prepared through recrystallization by dissolving some of the material in MeOH, diluting with EtOAc, and allowing slow evaporation of the solvent mixture. R_f = 0.7 (10% MeOH/CH_2Cl_2); ^{1}H NMR (400 MHz, $CDCl_3$) δ 8.60 (s, 1H), 8.47 (d, J = 3.8 Hz, 1H), 7.63 (dt, J = 7.9, 1.8, 1H), 7.22 (dd, J = 7.9, 4.8 Hz, 1H), 6.00 (dd, J = 7.9, 4.8 Hz, 1H), 3.69−3.58 (m, 1H), 3.13 (ddd, J = 13.6, 4.9, 2.2 Hz, 1H), 2.39−2.24 (m, 3H), 2.15−2.01 (m, 3H), 2.00−1.88 (m, 3H), 1.82 (qd, J = 10.9, 5.0 Hz, 1H), 1.73−1.54 (m, 4H), 1.49 (td, J = 12.2, 4.7 Hz, 1H), 1.20−1.06 (m, 2 H), 1.13 (s, 3H), 1.04 (s, 3H); ^{13}C NMR (101 MHz, $CDCl_3$) δ 159.2, 151.5, 148.2, 148.0, 133.9, 132.8, 129.1, 123.2, 119.1, 106.5, 70.6, 56.9, 49.3, 47.3, 40.5, 38.4, 36.5, 35.1, 33.7, 31.7, 30.8, 29.9, 20.8, 19.7, 16.6; IR (thin film) 3345, 2209 cm^{-1}; mp 232−235 °C (MeOH−EtOAc, dec); $[\alpha]_D^{23}$ −69.9 (c 1.00, $CHCl_3$); HRMS (ESI) m/z [M + H]$^+$ calcd for $C_{25}H_{31}N_2O$ 375.2431; found 375.2433; LCMS t_R = 4.38 min.

*3β-Hydroxy-17-(3-pyridyl)androsta-5,16-dien-6-carboxamide (**8**).* A 25 mL round-bottom flask was charged with **7** (99.9 mg, 0.267 mmol) and MeOH (13.5 mL). Pellets of NaOH (0.485 g, 11.5 mmol, 43.0 equiv) were added. Note: It was important to ensure that the NaOH is fully dissolved before continuing on to the next step. Then, a solution of H_2O_2 (30 wt %, 7.6 mL, 74 mmol, 280 equiv) was added dropwise over 5 min. Note: During the addition, the reaction mixture went from clear, colorless to cloudy, white, then back to clear, colorless. After stirring for 46 h, the reaction mixture was diluted with H_2O (10 mL), and the aqueous layer was extracted with CH_2Cl_2 (3 × 10 mL). The combined organic layers were concentrated. The crude product was purified by chromatography (50 g of C18 silica gel, H_2O containing 0.1 vol % NH_4OH to MeCN) to afford **8** (0.104 g, 0.264 mmol, 99% yield) as a white, amorphous solid. R_f = 0.4 (10% MeOH/CH_2Cl_2); ^{1}H NMR (400 MHz, $CDCl_3$) δ 8.60 (dd, J = 2.2, 6.0 Hz, 1H), 8.45 (dd, J = 4.8, 1.6 Hz, 1H), 7.63 (dt, J = 7.9, 2.0 Hz, 1H), 7.22 (ddd, J = 7.9, 4.8, 0.7 Hz, 1H), 5.99 (dd, J = 3.3, 1.8 Hz, 1H), 5.74 (s, 1H), 5.53 (s, 1H), 3.62−3.52 (m, 1H), 2.86 (ddd, J = 13.5, 4.7, 2.2 Hz, 1H), 2.38−2.23 (m, 2H), 2.22−2.13 (m, 1H), 2.12−1.76 (complex, 6H), 1.73−1.44 (complex, 7H), 1.19−1.05 (m, 1H), 1.11 (s, 3H), 1.04 (s, 3H); ^{13}C NMR (101 MHz, $CDCl_3$) δ 174.6, 151.6, 148.0, 147.9, 139.8, 133.9, 132.9, 129.3, 129.0, 123.2, 71.1, 57.3, 50.0, 47.4, 37.8, 37.01, 36.99, 35.3, 33.6, 31.9, 31.1, 30.1, 21.0, 19.6, 16.7; IR (thin film) 3321, 3180, 1646, 1600 cm^{-1}; mp 240−245 °C (dec); $[\alpha]_D^{22}$ −32.2 (c 1.00, MeOH); HRMS (ESI) m/z [M + H]$^+$ calcd for $C_{25}H_{33}N_2O_2$ 393.2537; found 393.2540; LCMS t_R = 3.23 min.

*3β-Acetoxy-6α-hydroxy-5α-androst-16-en-17-yl Trifluoromethanesulfonate (**9**).* A flame-dried 100 mL round-bottom flask was charged with **2** (3.00 g, 6.49 mmol) and anhydrous THF (32 mL) under Ar. The reaction mixture was cooled to 0 °C, and a solution of BH_3·THF (1 M in THF, 6.8 mL, 6.80 mmol, 1.05 equiv) was added dropwise over 10 min. After stirring for 4 h at 0 °C, H_2O (11 mL) was added slowly dropwise. **CAUTION:** A single drop of H_2O results in rapid gas evolution! Then, $NaBO_3$·$4H_2O$ (1.11 g, 7.18 mmol, 1.1 equiv) was added in one portion, and the reaction mixture was allowed to warm slowly to rt. After stirring for 18 h, the reaction mixture was filtered, and the precipitate was rinsed with small portions of THF (3 × 20 mL). The combined organic layers were washed with brine (60 mL), dried over Na_2SO_4, filtered, and concentrated. The crude product was purified by chromatography (80 g of silica gel, 0−35% EtOAc/hexanes) to afford **9** (0.871 g, 1.81 mmol, 28% yield) as a white, foamy solid and recovered **2** (1.17 g, 2.52 mmol, 39%). An analytical sample was prepared through recrystallization by dissolving some of the material in Et_2O, diluting with hexanes, and allowing slow evaporation of the solvent mixture. R_f = 0.1 (25% EtOAc/hexanes); ^{1}H NMR (400 MHz, $CDCl_3$) δ 5.57 (dd, J = 3.3, 1.7 Hz, 1H), 4.73−4.61 (m, 1H), 3.44 (td, J = 10.5, 4.3 Hz, 1H), 2.28−2.16 (m, 2H), 2.05−1.96 (m, 2H), 2.03 (s, 3H), 1.91−1.79 (m, 1H), 1.77−1.54 (complex, 5H), 1.53−1.24 (complex, 5H), 1.16−1.04 (m, 2H), 1.01−0.90 (m, 1H), 0.96 (s, 3H), 0.87 (s, 3H), 0.85−0.79 (m, 1H); ^{13}C NMR (101 MHz, $CDCl_3$) δ 170.6, 159.0, 118.5 (q, J = 320 Hz), 114.4, 73.3, 69.1, 54.0, 53.8, 51.8, 44.8, 40.4, 36.7, 36.4, 32.5, 32.3, 28.5, 28.3, 27.1, 21.4, 20.4, 25.2, 13.2; ^{19}F NMR (376 MHz, $CDCl_3$) δ − 73.6 (s); IR (neat) 3532, 1715, 1625 cm^{-1}; mp 136−139 °C (Et_2O−hexanes); $[\alpha]_D^{23}$ +25.4 (c 1.00, $CHCl_3$); HRMS (APCI) m/z [M − CH_3CO_2]$^+$ calcd for $C_{22}H_{32}F_3O_6S$ 421.1655; found 421.1649.

*6α-Hydroxy-17-(3-pyridyl)-5α-androst-16-en-3β-yl Acetate (**10a**).* Following general procedure A, **9** (0.676 g, 1.41 mmol) was coupled to 3-(diethylboranyl)pyridine (0.235 g, 1.60 mmol, 1.1 equiv) using bis(triphenylphosphine)palladium(II) dichloride (0.100 g, 0.143 mmol, 0.1 equiv) in anhydrous THF (8.3 mL) and a saturated solution of $NaHCO_3$ (2.8 mL) for 23 h. After workup, the crude product was purified by chromatography (24 g of silica gel, 0−50% EtOAc/hexanes) to afford mostly pure **10a** (0.465 g), which was recrystallized from MeOH−H_2O to give a white, crystalline solid (0.282 g, 0.690 mmol, 49% yield). R_f = 0.2 (50% EtOAc/hexanes); ^{1}H NMR (400 MHz, $CDCl_3$) δ 8.59 (d, J = 1.8 Hz, 1H), 8.44 (dd, J = 4.8,

1.5 Hz, 1H), 7.62 (dt, J = 7.9, 1.9 Hz, 1H), 7.20 (ddd, J = 7.9, 4.8, 0.7 Hz, 1H), 5.97 (dd, J = 3.2, 1.7 Hz, 1H), 4.73−4.63 (m, 1H), 3.51−3.42 (m, 1H), 2.30−2.20 (m, 2H), 2.12−1.96 (m, 3H), 2.02 (s, 3H), 1.89−1.80 (m, 1H), 1.80−1.54 (complex, 5H), 1.53−1.27 (complex, 4H), 1.15−0.95 (m, 3H), 0.99 (s, 3H), 0.88 (s, 3H), 0.87−0.77 (m, 1H); ^{13}C NMR (101 MHz, $CDCl_3$) δ 170.7, 151.8, 148.02, 147.99, 133.8, 133.0, 129.2, 123.2, 73.6, 69.4, 57.2, 54.1, 52.0, 47.6, 41.6, 37.0, 36.6, 35.3, 33.0, 31.8, 28.5, 27.3, 21.5, 21.2, 16.8, 13.5; IR (neat) 3216, 1727 cm^{-1}; mp 211−214 °C (MeOH−H_2O); $[\alpha]_D^{22}$ +46.2 (c 1.00, $CHCl_3$); HRMS (ESI) m/z $[M + H]^+$ calcd for $C_{26}H_{36}NO_3$ 410.2690; found 410.2693.

*17-(3-Pyridyl)-5α-androst-16-en-3β,6α-diol (**10b**).* Following general procedure B, **10a** (60.4 mg, 0.147 mmol) was reacted with K_2CO_3 (0.203 g, 1.47 mmol, 9.9 equiv) in MeOH (4.9 mL) for 15 h. After workup, the crude product was purified by chromatography (4 g of silica gel, 0−10% MeOH/CH_2Cl_2) to afford **10b** (52.4 mg, 0.143 mmol, 97% yield) as a white, amorphous solid. An analytical sample was prepared by recrystallization from MeOH−H_2O. R_f = 0.6 (10% MeOH/CH_2Cl_2); ^{1}H NMR (400 MHz, DMSO-d_6) δ 8.58 (s, 1H), 8.43 (d, J = 3.9 Hz, 1H), 7.77−7.71 (m, 1H), 7.33 (dd, J = 7.8, 4.8 Hz, 1H), 6.11−6.07 (m, 1H), 4.44 (d, J = 4.5 Hz, 1H), 4.31 (d, J = 5.6 Hz, 1H), 3.29−3.11 (m, 2H), 2.18 (ddd, J = 15.7, 6.3, 3.2 Hz, 1H), 2.12−1.94 (m, 3H), 1.89 (dt, J = 12.2, 4.1 Hz, 1H), 1.70−1.46 (complex, 5H), 1.43−1.20 (m, 3H), 1.03−0.82 (complex, 4H), 0.97 (s, 3H), 0.78 (s, 3H), 0.75−0.66 (m, 1H); ^{13}C NMR (101 MHz, DMSO-d_6) δ 151.1, 147.8, 147.1, 133.3, 132.1, 128.9, 123.3, 69.6, 67.3, 56.9, 53.7, 51.6, 46.9, 41.5, 37.0, 35.9, 34.7, 32.4, 32.3, 31.3, 31.2, 20.7, 16.4, 13.2; IR (neat) 3451, 3192 cm^{-1}; mp 225−229 °C (MeOH−H_2O); $[\alpha]_D^{22}$ +54 (c 0.50, MeOH); HRMS (ESI) m/z $[M + H]^+$ calcd for $C_{24}H_{34}NO_2$ 368.2584; found 368.2583; LCMS t_R = 3.45 min.

*3β-Acetoxy-6-oxo-5α-androst-16-en-17-yl Trifluoromethanesulfonate (**11**).* A 100 mL round-bottom flask was charged with **9** (3.90 g, 8.12 mmol) and anhydrous CH_2Cl_2 (81 mL). The reaction mixture was cooled to 0 °C, and Dess−Martin periodinane (6.89 g, 16.2 mmol, 2.0 equiv) was added in one portion. Then, the reaction mixture was allowed to warm slowly to rt. After stirring for 16 h, a saturated solution of $Na_2S_2O_3$ (150 mL) was added, and the reaction mixture was stirred for 15 min. The aqueous layer was extracted with CH_2Cl_2 (2 × 75 mL). The combined organic layers were washed with a saturated solution of $NaHCO_3$ (200 mL), dried over $MgSO_4$, filtered, and concentrated. The crude product was purified by chromatography (80 g of silica gel, 0−25% EtOAc/hexanes) to afford **11** (3.46 g, 7.24 mmol, 89% yield) as a white, amorphous solid. An analytical sample was prepared through recrystallization by dissolving some of the material in Et_2O, diluting with hexanes, and allowing slow evaporation of the solvent mixture. R_f = 0.5 (25% EtOAc/hexanes); ^{1}H NMR (400 MHz, $CDCl_3$) δ 5.58 (dd, J = 3.1, 1.5 Hz, 1H), 4.67 (tt, J = 11.5, 4.7 Hz, 1H), 2.37−2.32 (m, 1H), 2.29 (dd, J = 12.7, 3.1 Hz, 1H), 2.20 (ddd, J = 14.9, 6.4, 3.3 Hz, 1H), 2.10−1.92 (complex, 4H), 2.03 (s, 3H), 1.90−1.73 (complex, 5H), 1.61−1.37 (complex, 5H), 1.31 (td, J = 13.5, 4.0 Hz, 1H), 0.97 (s, 3H), 0.80 (s, 3H); ^{13}C NMR (101 MHz, $CDCl_3$) δ 209.2, 170.7, 158.9, 118.7 (q, J = 321 Hz), 114.6, 72.7, 56.9, 54.3, 54.2, 45.4, 45.3, 41.1, 36.3, 35.9, 32.4, 28.5, 26.9, 26.2, 21.5, 21.0, 15.4, 13.2; ^{19}F NMR (376 MHz, $CDCl_3$) δ −73.6 (s); IR (thin film) 1713, 1627 cm^{-1}; mp 162−165 °C (Et_2O−hexanes); $[\alpha]_D^{23}$ −9.9 (c 1.00, $CHCl_3$); HRMS (APCI) m/z $[M - CH_3CO_2]^+$ calcd for $C_{22}H_{30}F_3O_6S$ 419.1498; found 419.1492.

*17-(3-Pyridyl)-6-oxo-5α-androst-16-en-3β-yl Acetate (**12a**).* Following general procedure A, **11** (3.20 g, 6.69 mmol) was coupled to 3-(diethylboranyl)pyridine (1.11 g, 7.57 mmol, 1.1 equiv) using bis(triphenylphosphine)palladium(II) dichloride (0.471 g, 0.671 mmol, 0.1 equiv) in anhydrous THF (40 mL) and a saturated solution of $NaHCO_3$ (13.3 mL) for 17 h. After workup, the crude product was purified by chromatography (80 g of silica gel, 0−50% EtOAc/hexanes) to afford **12a** (2.25 g, 5.51 mmol, 82% yield) as a white, amorphous solid. An analytical sample was prepared through recrystallization by dissolving some of the material in EtOAc, diluting with hexanes, and allowing slow evaporation of the solvent mixture. R_f = 0.3 (50% EtOAc/hexanes); ^{1}H NMR (400 MHz, $CDCl_3$) δ 8.58 (d, J = 2.2 Hz, 1H), 8.44 (dd, J = 4.8, 1.5 Hz, 1H), 7.61 (dt, J = 7.9, 2.0 Hz, 1H), 7.20 (dd, J = 7.9, 4.8 Hz, 1H), 5.95 (dd, J = 3.3, 1.7 Hz, 1H), 4.70−4.58 (m, 1H), 2.43−2.31 (m, 1H), 2.28 (dd, J = 12.7, 3.0 Hz, 1H), 2.19 (ddd, J = 15.8, 6.7, 3.4 Hz, 1H), 2.13−1.97 (complex, 4H), 2.00 (s, 3H), 1.96−1.89 (m, 1H), 1.88−1.69 (complex, 4H), 1.62−1.20 (complex, 6H), 0.98 (s, 3H), 0.80 (s, 3H); ^{13}C NMR (101 MHz, $CDCl_3$) δ 209.9, 170.7, 151.6, 148.2, 148.0, 133.8, 132.7, 128.9, 123.2, 72.8, 57.5, 56.8, 54.1, 47.9, 46.5, 41.1, 36.6, 36.3, 35.0, 31.6, 26.9, 26.6, 21.5, 21.4, 16.7, 13.2; IR (thin film) 1729, 1710 cm^{-1}; mp 159−164 °C (EtOAc−hexanes); $[\alpha]_D^{23}$ −6.2 (c 1.00, $CHCl_3$); HRMS (ESI) m/z $[M + H]^+$ calcd for $C_{26}H_{34}NO_3$ 408.2531; found 408.2533.

*3β-Hydroxy-17-(3-pyridyl)-5α-androst-16-en-6-one (**12b**).* Following general procedure B, **12a** (45.9 mg, 0.113 mmol) was reacted with K_2CO_3 (54.9 mg, 0.397 mmol, 3.5 equiv) in MeOH (3.7 mL) for 17 h. After workup, the crude product was purified by chromatography (4 g of silica gel, 0−5% MeOH/CH_2Cl_2) to afford **12b** (36.3 mg, 99.3 μmol, 88% yield) as a white, amorphous solid. R_f = 0.4 (5% MeOH/CH_2Cl_2); ^{1}H NMR (400 MHz, $CDCl_3$) δ 8.61 (s, 1H), 8.47 (d, J = 4.1 Hz, 1H), 7.63 (dt, J = 7.9, 2.0 Hz, 1H), 7.22 (dd, J = 7.8, 4.9 Hz, 1H), 5.98 (dd, J = 3.3, 1.7 Hz, 1H), 3.64−3.54 (m, 1H), 2.47−2.35 (m, 1H), 2.29−2.17 (m, 2H), 2.15−2.00 (complex, 4H), 1.97−1.73 (complex, 5H), 1.71−1.62 (m, 1H), 1.59−1.34 (complex, 5H), 1.32−1.22 (m, 1H), 1.01 (s, 3H), 0.82 (s, 3H); ^{13}C NMR (101 MHz, $CDCl_3$) δ 210.4, 151.6, 148.2, 148.0, 133.8, 132.8, 129.0, 123.2, 70.7, 57.6, 57.2, 54.3, 48.0, 46.6, 41.2, 36.6, 36.6, 35.1, 31.6, 30.8, 30.2, 21.6, 16.8, 13.4; IR (thin film) 3224, 1702 cm^{-1}; mp 207−212 °C; $[\alpha]_D^{22}$ −9.0 (c 1.00, $CHCl_3$); HRMS (ESI) m/z $[M + H]^+$ calcd for $C_{24}H_{32}NO_2$ 366.2476; found 366.2422; LCMS: t_R = 3.54 min.

*6-Hydroxyimino-17-(3-pyridyl)-5α-androst-16-en-3β-yl Acetate (**13a**).* Following general procedure C, **12a** (2.10 g, 5.15 mmol) was reacted with NH_2OH·HCl (2.50 g, 36.1 mmol, 7.0 equiv) and NaOAc (2.96 g, 36.1 mmol, 7.0 equiv) in EtOH (170 mL) and H_2O (1.35 mL) for 24 h. After workup, the crude product was purified by chromatography (80 g of silica gel, 0−5% MeOH/CH_2Cl_2) to afford **13a** (2.13 g, 5.04 mmol, 98% yield) as a white, amorphous solid. An analytical sample was prepared by recrystallization from MeOH−H_2O. R_f = 0.5 (5% MeOH/CH_2Cl_2); ^{1}H NMR (400 MHz, $CDCl_3$) δ 8.61 (d, J = 1.7 Hz, 1H), 8.47 (dd, J = 4.8, 1.4 Hz, 1H), 8.08 (s, 1H), 7.64 (dt, J = 8.0, 1.7 Hz, 1H), 7.22 (dd, J = 7.7, 4.9 Hz, 1H), 5.99 (dd, J = 3.2, 1.7 Hz, 1H), 4.75−4.64 (m, 1H), 3.43 (dd, J = 13.6, 4.3 Hz, 1H), 2.32 (ddd, J = 15.7, 6.4, 3.3 Hz, 1H), 2.20−2.11 (m, 1H), 2.10−1.97 (m, 3H), 2.03 (s, 3H), 1.91−1.69 (complex, 5H), 1.66−1.43 (complex, 4H), 1.42−1.32 (m, 1H), 1.30−1.17 (m, 1H), 1.14−1.06 (m, 1H), 1.01 (s, 3H), 0.84 (s, 3H); ^{13}C NMR (101 MHz, $CDCl_3$) δ 170.8, 159.4, 151.6, 148.1, 148.0, 133.9, 132.9, 129.2, 123.2, 73.4, 57.6, 54.6, 49.7, 47.9, 39.1, 35.9, 35.2, 34.4, 31.8, 29.5, 27.8, 27.2, 21.6, 21.5, 16.9, 12.7; IR (neat) 1727 cm^{-1}; mp 216−220 °C (MeOH−H_2O, dec); $[\alpha]_D^{22}$ −40.0 (c 1.00, $CHCl_3$); HRMS (ESI) m/z $[M + H]^+$ calcd for $C_{26}H_{35}N_2O_3$ 423.2642; Found 423.2633.

*3β-Hydroxy-17-(3-pyridyl)-5α-androst-16-en-6-one Oxime (**13b**).* Following general procedure C, **12b** (25.0 mg, 68.0 μmol) was reacted with NH_2OH·HCl (33.6 mg, 0.484 mmol, 7.1 equiv) and NaOAc (39.7 mg, 0.484 mmol, 7.1 equiv) in EtOH (2.3 mL) and H_2O (20 μL) for 17 h. After workup, the crude product was purified by chromatography (4 g of silica gel, 0−5% MeOH/CH_2Cl_2) to afford **13b** (21.5 mg, 56.5 μmol, 83% yield) as a white, amorphous solid. R_f = 0.2 (5% MeOH/CH_2Cl_2); ^{1}H NMR (400 MHz, DMSO-d_6) δ 10.39 (s, 1H), 8.58 (d, J = 4.3 Hz, 1H), 7.75 (d, J = 8.0 Hz, 1H), 7.33 (dd, J = 7.3, 5.3 Hz, 1H), 6.10 (s, 1H), 4.50 (d, J = 4.1 Hz, 1H), 3.25 (dd, J = 13.1, 3.0 Hz, 1H), 2.23 (d, J = 16.2 Hz, 1H), 2.12−1.88 (m, 3H), 1.82−1.72 (m, 1H), 1.70−1.58 (complex, 5H), 1.46−1.16 (complex, 6H), 1.14−1.01 (m, 2H), 0.96 (s, 3H), 0.69 (s, 3H); ^{13}C NMR (101 MHz, DMSO-d_6) δ 156.9, 151.0, 147.8, 147.2, 133.3, 132.0, 128.9, 123.4, 69.3, 56.9, 53.6, 49.0, 47.1, 38.2, 35.6, 34.5, 33.7, 31.9, 31.2, 30.9, 28.8, 21.0, 16.3, 12.3; IR (neat) 3277 cm^{-1}; mp 251−256 °C (dec); $[\alpha]_D^{23}$ −31 (c 0.50, 1,4-dioxane); HRMS (ESI) m/z $[M + H]^+$ calcd for $C_{24}H_{32}N_2O_2$ 381.2537; found 381.2534; LCMS t_R = 3.54 min.

*6-Aza-7-oxo-17-(3-pyridyl)-B-homo-5α-androst-16-en-3β-yl Acetate (**14a**).* A flame-dried 20 mL vial was charged with **13b** (0.101 g, 0.239 mmol) and anhydrous THF (5 mL) under Ar. The reaction

mixture was cooled to 0 °C, and $SOCl_2$ (60.0 μL, 8.22 mmol, 35.0 equiv) was added dropwise over 5 min. After stirring for 4 h at 0 °C, the reaction mixture was quenched by slow addition of H_2O (2 mL). The reaction mixture was allowed to warm to rt, neutralized with a saturated solution of $NaHCO_3$ (25 mL), and diluted with CH_2Cl_2 (10 mL). The organic layer was separated, and the aqueous layer was extracted with CH_2Cl_2 (3 × 5 mL). The combined organic layers were dried over $MgSO_4$, filtered, and concentrated. The crude product was purified by chromatography (12 g of silica gel, 0−2.5% MeOH/CH_2Cl_2) to afford **14a** (44.7 mg, 0.106 mmol, 45% yield) as a white, amorphous solid. R_f = 0.6 (10% MeOH/CH_2Cl_2); ^{1}H NMR (400 MHz, $CDCl_3$) δ 8.59 (s, 1H), 8.47−8.39 (m, 1H), 7.61 (d, *J* = 7.9 Hz, 1H), 7.21 (dd, *J* = 7.9, 4.8 Hz, 1H), 5.99−5.93 (m, 1H), 5.46 (s, 1H), 4.70−4.59 (m, 1H), 3.46 (dt, *J* = 12.2, 5.1 Hz, 1H), 2.40−2.30 (m, 3H), 2.19 (ddd, *J* = 15.8, 11.5, 1.8 Hz, 1H), 2.08−1.95 (complex, 6H), 1.95−1.79 (m, 3H), 1.69 (td, *J* = 11.5, 6.6 Hz, 1H), 1.57−1.32 (complex, 4H), 1.18−1.04 (m, 2H), 1.01 (s, 3H), 0.91 (s, 3H); ^{13}C NMR (101 MHz, $CDCl_3$) δ 176.0, 170.5, 151.5, 148.2, 147.9, 133.8, 132.6, 128.6, 123.2, 70.9, 59.0, 57.0, 56.7, 47.2, 40.6, 39.0, 35.5, 35.4, 34.7, 33.1, 33.0, 27.1, 22.9, 21.4, 16.5, 12.5; IR (neat) 3231, 1722, 1666 cm^{-1}; mp 248−252 °C; $[\alpha]_D^{22}$ +49.7 (*c* 1.00, $CHCl_3$); HRMS (ESI) *m*/*z* $[M + H]^+$ Calcd for $C_{26}H_{35}N_2O_3$ 423.2642; Found 423.2633.

6-Aza-7-oxo-17-(3-pyridyl)-B-homo-5α-androst-16-en-3β-ol (14b). Following general procedure B, **14a** (47.1 mg, 0.111 mmol) was reacted with K_2CO_3 (0.154 g, 1.13 mmol, 10.1 equiv) in MeOH (3.7 mL) for 17 h. After workup, the crude product was purified by chromatography (4 g of silica gel, 0−5% MeOH/CH_2Cl_2) to afford **14b** (42.4 mg, 0.111 mmol, 100%) as a white, amorphous solid. R_f = 0.5 (5% MeOH/CH_2Cl_2); ^{1}H NMR (400 MHz, $CDCl_3$) δ 8.59 (s, 1H), 8.46 (s, 1H), 7.64 (dt, *J* = 8.0, 1.9 Hz, 1H), 7.23 (dd, *J* = 8.0, 4.8 Hz, 1H), 5.98 (dd, *J* = 3.4, 1.8 Hz, 1H), 5.34 (d, *J* = 5.3 Hz, 1H), 3.66−3.56 (m, 1H), 3.44−3.35 (m, 1H), 2.37 (d, *J* = 6.9 Hz, 1H), 2.33 (dd, *J* = 6.6, 3.4 Hz, 1H), 2.25−2.07 (m, 2H), 2.07−1.89 (complex, 4H), 1.88−1.76 (m, 2H), 1.68 (td, *J* = 11.5, 6.6 Hz, 1H), 1.59−1.17 (complex, 5H), 1.13−1.04 (m, 2H), 1.02 (s, 3H), 0.91 (s, 3H); ^{13}C NMR (101 MHz, $CDCl_3$) δ 176.0, 151.5, 147.9, 147.6, 134.1, 132.8, 128.8, 123.3, 68.8, 59.1, 57.3, 56.8, 47.2, 40.7, 39.0, 38.8, 35.7, 35.6, 33.2, 33.0, 31.0, 22.9, 16.6, 12.5; IR (thin film) 3234, 1648 cm^{-1}; mp 271−274 °C (dec); $[\alpha]_D^{22}$ +45 (*c* 0.95, $CHCl_3$); HRMS (ESI) *m*/*z* $[M + H]^+$ calcd for $C_{24}H_{33}N_2O_2$ 381.2537; found 381.2544; LCMS t_R = 2.90 min.

17-Oxoandrost-5-en-3β-yl Acetate (15)..[28−30] A 20 mL microwave vial was charged with 17-oxoandrost-5-en-3β-ol (10.0 g, 34.7 mmol), *p*-TsOH·H_2O (67.7 mg, 0.356 mmol, 0.01 equiv), and Ac_2O (13.0 mL, 111 mmol, 4.0 equiv). The suspension was stirred at 80 °C for 12 min using a microwave reactor (time measured when the reaction mixture reached the programmed temperature after a ramp period of ca. 1 min). After cooling to rt, the resulting wet solid was dissolved in CH_2Cl_2 (200 mL), and a saturated solution of $NaHCO_3$ (200 mL) was added slowly. The mixture was stirred for 15 h to hydrolyze any remaining Ac_2O. After the organic layer was separated, the aqueous layer was extracted with CH_2Cl_2 (3 × 50 mL). The combined organic layers were washed with brine (100 mL), dried over $MgSO_4$, filtered, and concentrated to afford **15** (11.3 g, 34.2 mmol, 99% yield) as a white, amorphous solid, which was used without further purification. R_f = 0.6 (25% EtOAc/hexanes); ^{1}H NMR (400 MHz, $CDCl_3$) δ 5.40 (d, *J* = 5.2 Hz, 1H), 4.65−4.55 (m, 1H), 2.46 (dd, *J* = 19.2, 8.8 Hz, 1H), 2.39−2.25 (m, 2H), 2.16−2.05 (m, 2H), 2.03 (s, 3H), 1.99−1.81 (complex, 4H), 1.72−1.63 (m, 3H), 1.63−1.42 (m, 3H), 1.34−1.24 (m, 2H), 1.20−1.09 (m, 1H), 1.04 (s, 3H), 1.03−0.98 (m, 1H), 0.88 (s, 3H); ^{13}C NMR (101 MHz, $CDCl_3$) δ 221.2, 170.6, 140.1, 122.0, 73.9, 51.8, 50.3, 47.7, 38.2, 37.1, 36.9, 36.0, 31.6, 31.5, 30.9, 27.8, 22.0, 21.6, 20.5, 19.5, 13.7; IR (neat) 1723, 1737 cm^{-1}; mp 169−171 °C, lit.[28] 167−170 °C; $[\alpha]_D^{23}$ −4.2 (*c* 1.00, $CHCl_3$), lit.[29] $[\alpha]_D^{18}$ −3.1 (*c* 1.00, $CHCl_3$); HRMS (APCI) *m*/*z* $[M - CH_3CO_2]^+$ calcd for $C_{19}H_{27}O$ 271.2056; found 271.2054.

Plasmid Constructs. Recombinantly expressed human cytochrome P450 enzymes CYP17A1, CYP21A2, and human full-length NADPH cytochrome P450 reductase enzymes were used in this study. The gene for each P450 protein was constructed synthetically with codon optimization for expression in *E. coli* and modified to omit the single, N-terminal transmembrane helix, and a C-terminal histidine tag was added. Specifically, the 17A1Δ19H construct is as described.[16] The CYP21A2dH construct omitted the N-terminal 2−19 residues, substituted the sequence coding for 20-NWWKLRSLH-28 with nucleotides coding for AKKTSSKGK, and added codons for a C-terminal four histidine tag immediately prior to the stop codon. Each cytochrome P450 gene was inserted into the pCWori+ vector, which confers carbenicillin resistance. A synthetic, codon-optimized gene of human full-length NADPH-cytochrome P450 reductase in pET-29a(+) is as described.[31]

Expression and Purification of CYP17A1, CYP21A2, and NADPH-cytochrome P450 Reductase Enzymes. *E. coli* DH5α cells already harboring the pGro7 plasmid for chaperone expression (chloramphenicol resistance) were transformed with either the pCW17A1Δ19H or pCW21A2dH plasmids and grown on lysogeny broth (LB) agar plates containing chloramphenicol (20 μg/mL) and carbenicillin (100 μg/mL). A single colony was first grown in 5 mL of LB media at 37 °C, 250 rpm in the presence of antibiotics until $O.D._{600}$ = 0.6. Then 100 μL of this primary culture was inoculated into 20 mL of LB media and grown at 37 °C, 250 rpm for ca. 12 h, after which 20 mL was used to inoculate 1 L of Terrific Broth (TB) media in a 2.8 L Fernbach flask. This culture was then grown at 37 °C, 250 rpm until $O.D._{600}$ = 0.5. At this point, chaperone expression was induced by the addition of L-arabinose (1 g). The heme precursor δ-aminolevulinic acid (132 mg) also added. The temperature was then reduced to 27 °C, and the culture was allowed to continue growing until the $O.D._{600}$ reached 0.8. At this point, the expression of P450 protein was induced by the addition of 0.8 mM IPTG. Temperature and shaking were reduced to 25 °C and 200 rpm, respectively. Cultures were harvested after 48 h, and cells were collected by centrifugation at 8000*g* for 10 min. Cells were resuspended in 25 mL of buffer (100 mM potassium phosphate, pH 7.4, 300 mM NaCl, and 20% (v/v) glycerol for CYP17A1; 100 mM potassium phosphate, pH 6.8, 300 mM NaCl, and 20% glycerol for CYP21A2) per liter of *E. coli* culture and stored at −80 °C until purification.

CYP17A1 protein was purified as described[14] with the following modifications. A French press was used for cell disruption, and protein was extracted from the membrane using 2% (v/v) Emulgen-913 (Desert Biologicals) for 60 min. Cell lysate was centrifuged at 100,000*g* for 1 h to remove membranes, and the resulting P450-containing supernatant was loaded on a 30 mL Ni-NTA Agarose (Qiagen) column pre-equilibrated with Ni buffer (100 mM potassium phosphate, pH 7.4, 300 mM NaCl, 20% (v/v) glycerol, and 0.2% (v/v) Emulgen-913). This column was subsequently washed with 3 column volumes (CV) of Ni buffer, followed by 6 CV of Ni buffer supplemented with 100 mM glycine, and eluted using 4 CV of Ni buffer supplemented with 100 mM glycine and 80 mM histidine. Elution fractions were pooled based on absorbance at 417 nm, diluted 5−6-fold in CM buffer (5 mM potassium phosphate, pH 7.4, 20% (v/v) glycerol, and 100 mM glycine), supplemented with 0.2% (v/v) Emulgen-913, and loaded onto a 5 mL carboxymethyl sepharose fast-flow column (GE Healthcare) previously equilibrated with CM buffer. The column was washed with 20 CV of CM buffer and eluted with CM elution buffer (50 mM potassium phosphate, pH 7.4, 500 mM NaCl, 100 mM glycine, and 20% (v/v) glycerol). Fractions were pooled based on absorbance at 417 nm, concentrated to 4 mL, and loaded on a size exclusion chromatography column (HiLoad 16/60 Superdex 200) equilibrated with buffer CM elution buffer.

Purification of CYP21A2 involved cell disruption by French press, followed by membrane protein extraction with 2% (v/v) Emulgen-913 (Desert Biologicals) for 90 min, and ultracentrifugation (100,000*g* for 1 h) to pellet the membranes. The resulting supernatant containing CYP21A2 was loaded onto 30 mL of Ni-NTA Agarose resin pre-equilibrated with Ni buffer (100 mM potassium phosphate, pH 6.8, 300 mM NaCl, 20% (v/v) glycerol, 1 mM BME, and 0.2% (v/v) Emulgen-913). The column was subsequently washed with 3 CV of Ni buffer, followed by 6 CV of Ni buffer supplemented with 10 mM histidine, and eluted using 4 CV of Ni buffer supplemented with 80 mM histidine. Elution fractions were pooled based on absorbance at

417 nm, diluted 5−6-fold in CM buffer (10 mM potassium phosphate, pH 6.8, 20% (v/v) glycerol, and 1 mM BME), supplemented with 0.2% (v/v) Emulgen-913, and loaded onto a 5 mL carboxymethyl sepharose fast-flow column previously equilibrated with CM buffer. The column was washed with 20 CV of CM buffer and eluted with CM elution buffer (50 mM potassium phosphate, pH 6.8, 350 mM NaCl, and 20% (v/v) glycerol). Fractions were pooled based on absorbance at 417 nm, concentrated to 4 mL, and loaded on a size exclusion chromatography column equilibrated with buffer CM elution buffer.

The purity, quality, and quantity of P450 proteins were assessed by the UV−vis spectrum, SDS-PAGE, and the reduced carbon monoxide difference spectrum. Concentration of P450 enzyme was determined from the reduced carbon monoxide difference spectra in the presence of 2 μM progesterone as a ligand.

Human full-length NADPH-cytochrome P450 reductase (CPR) enzyme was expressed and purified as described.[31] Final reductase samples were evaluated on SDS-PAGE and by UV−visible spectroscopy. CPR was quantitated by flavin absorbance of the fully oxidized protein at 454 nm.

Inhibition of Progesterone Hydroxylation. Abiraterone analogs were evaluated for their selectivity in inhibiting progesterone hydroxylation by CYP17A1 (17α-hydroxylation) vs CYP21A2 (21-hydroxylation). Initial stocks (10 mM) were made of each compound in DMSO. This stock was then serially diluted with DMSO to yield a concentration range of 0.3125 nM to 40.960 μM. Compound **3b** was further diluted to 0.0195 nM. Abiraterone itself was used as a reference inhibitor to assess structural changes altering selectivity in inhibition of CYP17A1 vs CYP21A2.

Progesterone hydroxylation was evaluated at the K_m for each enzyme under conditions where substrate utilization was <3%. Progesterone 17α-hydroxylation was evaluated by incubating CYP17A1 (20 pmol) with CPR (80 pmol) for 20 min at rt before combination with reaction buffer (50 mM Tris-HCl, pH 7.4, 5 mM $MgCl_2$) containing 6 μM progesterone. Equal volumes of serial diluted inhibitor stocks were added to yield a range of inhibitor concentrations with a constant final DMSO concentration (0.4%) across all reactions. Samples containing enzyme, substrate, and inhibitor were incubated for 3 min in a 37 °C water bath, and reactions were initiated by addition of 1 mM NADPH. Total reaction volume was 500 μL. Reactions were continued at 37 °C for 10 min and subsequently stopped by adding 200 mL of trichloroacetic acid (20%). Precipitated protein was cleared by centrifugation. Progesterone 21-hydroxylase inhibition assays were accomplished similarly using CYP21A2 (1 pmol) and CPR (4 pmol) with 0.3 μM progesterone substrate and an 8 min reaction time.

All samples were processed using the following protocol to quantitate hydroxylated progesterone by LC−MS/MS. Portions of the progesterone 17α-hydroxylation reaction samples (20 μL) and 21-hydroxylation reaction samples (100 μL) were mixed with 200 μL of HPLC-grade water in a sample vial, respectively. Deuterated progesterone-d_9 (CDN isotopes) was then added as an internal standard (12.5 pg). Samples were then extracted by adding 1 mL of MTBE, vortexing for 4 min, and permitting phase separation for 5 min. The bottom aqueous layer was removed by pipetting and the upper organic layer dried using a speedvac. Finally, dried samples were reconstituted with MeOH/H_2O (1:1), and 10 μL was injected on a Kinetex 50 × 2.1 mm, 3 μm particle size biphenyl column (Phenomenex) running on an Agilent 1260/1290 binary pump HPLC. Components were resolved using a gradient elution of ammonium fluoride (0.2 mM) in H_2O (mobile phase A) and 0.2 mM ammonium fluoride in MeOH (mobile phase B) with 60−100% mobile phase B gradient. Analytes were further directed into an Agilent 6495 triple quadrupole mass spectrometer using electrospray ionization in positive ionization mode and analyzed using multiple reaction monitoring mode.[32] Mass transitions 315.2 > 97.0 and 324.1 > 100.1 were used to monitor and quantify progesterone and the progesterone-d_9 internal standard, respectively, while 17α-hydroxyprogesterone and 21-hydroxyprogesterone were monitored and quantified using the 331.2 > 109 mass transition. The peak areas for specific analytes were determined using the Agilent MassHunter quantitative analysis program.

Inhibitory concentration (IC_{50}) for compounds were determined from two independent replicates (n = 2). Raw data was converted into % maximal activity and fitted with nonlinear regression (inhibitor vs response) using eq 1 and automatic outlier elimination (ROUT coefficient, Q = 5%)[33] in Prism (GraphPad Software, La Jolla, CA) and is presented as mean ± standard error.

$$Y = \min + \frac{(\max - \min)}{1 + 10^{(\log IC50 - x)\text{Hill slope}}} \quad (1)$$

CYP3A4 and CYP2D6 Inhibition Assays. Abiraterone and analog **13b** (5α-H, 6-oxime) were evaluated for inhibition of CYP3A4-mediated metabolism of luciferin isopropyl alcohol (Promega) and CYP2D6-mediated dextromethorphan metabolism, at substrate concentrations equivalent to their respective K_m values. Like CYP17A1 and CYP21A2, CYP3A4 and CYP2D6 were the recombinant, N-terminally truncated and C-terminally His-tagged enzymes that had been highly purified.[31] For CYP3A4, 10 pmol of CYP3A4, 40 pmol of CPR, and 10 pmol of cytochrome b_5 were combined in 100 mM potassium phosphate, pH 7.4. Inhibitors (0.04−0.64 μM, in EtOH or DMSO) were added, with a final solvent concentration of 0.4% in all reactions. A 25 μL aliquot of the protein, substrate, and inhibitor mixture was added into each well of flat-bottom 96-well plate (Corning Inc.). Using the GloMax Discover plate reader (Promega), plates were incubated for 3 min at 37 °C, followed by the addition of 25 μL of NADPH (200 μM) with shaking at 37 °C for 2 s after each addition to initiate the reaction. Reactions continued for 30 min at 37 °C and then were terminated, and product was converted to its luminescent form by the addition of esterase-containing luciferin detection reagent (50 μL). Finally, the plate was incubated at 37 °C for 20 min before luminescence was read. Each data point was generated in triplicate. To evaluate CYP2D6 inhibition, an assay was performed as described for dextromethorphan conversion to dextrophan without cytochrome b_5,[31] employing only minor changes. Inhibitor stocks (0.020−80 μM) were prepared as described above for the CYP3A4 assay. Substrate and product were separated using an isocratic flow of 40% mobile phase A, consisting of 10 mM potassium phosphate at pH 3.5, and 60% mobile phase B, consisting of 50% MeCN/100% MeOH in a 250/200 v/v ratio. Each sample was prepared in duplicate. Data from both assays was fit using Prism to determine the IC_{50} values as described for the progesterone hydroxylation assay.

X-ray Crystallography. Several analogs were cocrystallized with human CYP17A1, and structures were determined using previously reported methods.[16] Briefly, CYP17A1 in 50 mM Tris-HCl, pH 7.4, 20% glycerol, and 100 mM glycine was exchanged with the same buffer containing 10 μM of the desired inhibitor multiple times. The saturated CYP17A1 was then concentrated such that the final stock was ca. 30 mg/mL and 0.5% Emulgen 913. This protein/ligand complex (1 μL) was mixed 1:1 with precipitant solution consisting of 0.175 M Tris, pH 8.5 containing 30% PEG 3350, 3% glycerol, and 0.250−0.275 M lithium sulfate for the C6 oxime. For the C6 nitrile and C6 amide analogs, PEG was increased to 35%. Using hanging drop vapor diffusion, these drops were equilibrated against 750 μL of the same precipitant solution at 20 °C (C6 oxime) or 4 °C (C6 nitrile and C6 amide). Rod-shaped crystals grew in ca. 24 h and were cryoprotected using a 7:3 mixture of precipitant and 80% glycerol. X-ray diffraction data collected at Stanford Synchrotron Radiation Lightsource on beamline 12−2 was processed using XDS[34] and Scala.[35] Structures were solved by molecular replacement using a search model of CYP17A1 with galeterone (PDB 3SWZ)[16] and Phaser[36] in Phenix.[37] Model building and refinement were performed with COOT[38] and phenix.refine,[37] respectively. The coordinates for the three new X-ray crystallographic structures with compound **7**, **8**, and **13b** have been deposited to the Protein Data Bank under the identifiers 6CIZ, 6CHI, and 6CIR, respectively. Data collection and refinement statistics are provided in Table S1 (Supporting

Information). All protein structure figures were generated with Pymol.[39]

Computational Docking. Test compounds, with the exception of **3b** and **14b**, were each docked onto the crystal structures of CYP17A1 and CYP21A2 to analyze the potential binding mode, binding energy, and favorable or unfavorable interactions. All docking procedures were performed using various modules of Schrödinger Maestro suite (Schrödinger, LLC, New York, NY, 2017). The X-ray crystal structures of CYP17A1 with abiraterone (PDB 3RUK) and CYP21A2 with progesterone (PDB 4Y8W) were retrieved from RCSB PDB database, and atoms of chain A including heme and the associated ligand were preserved for docking. The polypeptide structures of CYP17A1 and CYP21A2 were optimized and prepared for docking using the Maestro Protein Preparation Wizard to assess bond order and missing hydrogens, followed by energy minimization using the OPLS3 force field. Gaps in the protein structures were not corrected as they were far from the active site. Water molecules were removed from the protein. The heme iron was assigned an oxidation state of +3. The Maestro Receptor Grid Generation module was then used to define a 15 × 15 × 15 Å grid from the center of the cocrystallized steroid ligands. Ligands used in the computational docking study were built by modifying the abiraterone structure (PDB 3RUK) using the Maestro 3D Build module. The Maestro LigPrep module was then used to generate conformers of each compound subjected to energy minimization using the OPLS3 force field protocol. The resulting compounds were docked into the prepared CYP17A1 and CYP21A2 structures using the Maestro Glide module. Docking was performed with standard precision with flexible ligand sampling. Ligands were constrained to within 10 Å of the iron. A total of 5000 initial poses were generated for each compound. Based on the pose score, the top 400 were selected and subjected to energy minimization using the OPLS3 force field. Finally, the top ten poses per compound were generated and ranked according to Glide score, which is an approximation of binding energy defined by receptor−ligand complex energies. The top pose was analyzed and presented in Results and Discussion.[40] In addition, the total free energy of binding ΔG_{bind} (kcal/mol) was determined for these poses using prime molecular mechanics energies combined with the generalized Born and surface area continuum solvation.[41] Residues within 8 Å from the ligand were defined as flexible during free energy calculation. This docking procedure was validated by docking abiraterone and progesterone to CYP17A1 and CYP21A2, respectively. Abiraterone docked into CYP17A1 with the highest Glide score was compared to abiraterone in the X-ray crystallographic structure, while progesterone docked into CYP21A2 was compared with the crystal structure of CYP21A2 bound to progesterone.

■ ASSOCIATED CONTENT

Supporting Information

The Supporting Information is available free of charge on the ACS Publications website at DOI: 10.1021/acs.jmedchem.8b00419.

IC_{50} determination, details of X-ray crystallography, and copies of ^{1}H and ^{13}C NMR spectra for some resynthesized and all new compounds (PDF)

SMILES strings (CSV)

PDB coordinates of **13b** docked into CYP17A1 (PDB) and CYP21A2 (PDB), **12b** docked into CYP17A1 (PDB) and CYP21A2 (PDB), **10b** docked into CYP17A1 (PDB) and CYP21A2 (PDB), **7** docked into CYP17A1 (PDB) and CYP21A2 (PDB), **8** docked into CYP17A1 (PDB) and CYP21A2 (PDB), **1b** docked into CYP17A1 (PDB) and CYP21A2 (PDB), and **6b** docked into CYP17A1 (PDB) and CYP21A2 (PDB)

Accession Codes

The coordinates for the three new X-ray crystallographic structures with compound **7**, **8**, and **13b** have been deposited to the Protein Data Bank under the identifiers 6CIZ, 6CHI, and 6CIR, respectively.

■ AUTHOR INFORMATION

Corresponding Authors

*E-mail: jaube@unc.edu.

*E-mail: scottee@umich.edu.

ORCID

Jeffrey Aubé: 0000-0003-1049-5767

Present Address

⊥Department of Chemistry, Cambridge University, Cambridge, England.

Author Contributions

C.F., C.D.V., and R.Y. contributed equally to this project. C.F. initially designed and produced many of the abiraterone analogs, undertook preliminary assays, analyzed data, and participated in crystallization and X-ray structure determination. C.D.V. resynthesized, characterized, and expanded the initial set of abiraterone analogs and analyzed data. R.Y. expressed and purified CYP17A1, CYP21A2, and NADPH-cytochrome P450 reductase recombinant proteins for assays, determined all IC_{50} values, performed the docking calculations, and analyzed data. K.L. resynthesized particular analogs. J.A. and E.E.S. conceived the study and analyzed data. The initial draft of the paper was written by C.D.V., R.Y., E.E.S., and J.A.; all authors participated in revision.

Notes

The authors declare no competing financial interest.

■ ACKNOWLEDGMENTS

We thank Patrick Porubsky, who helped develop an initial GC−MS method for steroid analysis; Linda Blake, who designed the CYP21A2 expression construct and developed the original expression and purification protocols; Natasha DeVore and Elyse Petrunak, who expressed CYP17A1 for crystallography while mentoring C.F. and worked with C.F. on crystallization and early structure determination; Patrick O'Day, who optimized LC−MS/MS methods for the final steroid analysis method used; and Brandie M. Ehrmann for LC−MS and MS data acquisition. This work was supported by National Institute of General Medical Sciences (R01 GM102505, to E.E.S. and J.A., and R37 GM076343, to E.E.S.), the University of North Carolina at Chapel Hill, and the University of Michigan—Ann Arbor. The content of this publication is solely the responsibility of the authors and does not necessarily represent the official views of NIH.

■ ABBREVIATIONS

CYP, cytochrome P450; CV, column volume

■ REFERENCES

(1) American Cancer Society. Cancer Facts & Figures 2017. https://www.cancer.org/research/cancer-facts-statistics/all-cancer-facts-figures/cancer-facts-figures-2017.html (accessed Jan 24, 2018).

(2) Geller, J. Basis for Hormonal Management of Advanced Prostate Cancer. *Cancer* **1993**, *71*, 1039−1045.

(3) Vogiatzi, P.; Claudio, P. P. Efficacy of Abiraterone Acetate in Post-docetaxel Castration-resistant Prostate Cancer. *Expert Rev. Anticancer Ther.* **2010**, *10*, 1027−1030.

(4) de Bono, J. S.; Logothetis, C. J.; Molina, A.; Fizazi, K.; North, S.; Chu, L.; Chi, K. N.; Jones, R. J.; Goodman, O. B., Jr.; Saad, F.; Staffurth, J. N.; Mainwaring, P.; Harland, S.; Flaig, T. W.; Hutson, T.

E.; Cheng, T.; Patterson, H.; Hainsworth, J. D.; Ryan, C. J.; Sternberg, C. N.; Ellard, S. L.; Flechon, A.; Saleh, M.; Scholz, M.; Efstathiou, E.; Zivi, A.; Bianchini, D.; Loriot, Y.; Chieffo, N.; Kheoh, T.; Haqq, C. M.; Scher, H. I. Abiraterone and Increased Survival in Metastatic Prostate Cancer. *N. Engl. J. Med.* **2011**, *364*, 1995−2005.

(5) Fizazi, K.; Scher, H. I.; Molina, A.; Logothetis, C. J.; Chi, K. N.; Jones, R. J.; Staffurth, J. N.; North, S.; Vogelzang, N. J.; Saad, F.; Mainwaring, P.; Harland, S.; Goodman, O. B., Jr.; Sternberg, C. N.; Li, J. H.; Kheoh, T.; Haqq, C. M.; de Bono, J. S. Abiraterone Acetate for Treatment of Metastatic Castration-resistant Prostate Cancer: Final Overall Survival Analysis of the COU-AA-301 Randomised, Double-Blind, Placebo-controlled Phase 3 Study. *Lancet Oncol.* **2012**, *13*, 983−992.

(6) Handratta, V. D.; Vasaitis, T. S.; Njar, V. C. O.; Gediya, L. K.; Kataria, R.; Chopra, P.; Newman, D.; Farquhar, R.; Guo, Z.; Qiu, Y.; Brodie, A. M. H. Novel C-17-Heteroaryl Steroidal CYP17 Inhibitors/Antiandrogens: Synthesis, in Vitro Biological Activity, Pharmacokinetics, and Antitumor Activity in the LAPC4 Human Prostate Cancer Xenograft Model. *J. Med. Chem.* **2005**, *48*, 2972−2984.

(7) Njar, V. C. O.; Brodie, A. M. H. Discovery and Development of Galeterone (TOK-001 or VN/124−1) for the Treatment of All Stages of Prostate Cancer. *J. Med. Chem.* **2015**, *58*, 2077−2087.

(8) Yamaoka, M.; Hara, T.; Hitaka, T.; Kaku, T.; Takeuchi, T.; Takahashi, J.; Asahi, S.; Miki, H.; Tasaka, A.; Kusaka, M. Orteronel (TAK-700), a Novel Non-Steroidal 17,20-Lyase Inhibitor: Effects on Steroid Synthesis in Human and Monkey Adrenal Cells and Serum Steroid Levels in Cynomolgus Monkeys. *J. Steroid Biochem. Mol. Biol.* **2012**, *129*, 115−128.

(9) Rafferty, S. W.; Eisner, J. R.; Moore, W. R.; Schotzinger, R. J.; Hoekstra, W. J. Highly-selective 4-(1,2,3-Triazole)-based P450C17A 17,20-Lyase Inhibitors. *Bioorg. Med. Chem. Lett.* **2014**, *24*, 2444−2447.

(10) Huang, A.; Jayaraman, L.; Fura, A.; Vite, G. D.; Trainor, G. L.; Gottardis, M. M.; Spires, T. E.; Spires, V. M.; Rizzo, C. A.; Obermeier, M. T.; Elzinga, P. A.; Todderud, G.; Fan, Y.; Newitt, J. A.; Beyer, S. M.; Zhu, Y.; Warrack, B. M.; Goodenough, A. K.; Tebben, A. J.; Doweyko, A. M.; Gold, D. L.; Balog, A. Discovery of the Selective CYP17A1 Lyase Inhibitor BMS-351 for the Treatment of Prostate Cancer. *ACS Med. Chem. Lett.* **2016**, *7*, 40−45.

(11) Attard, G.; Reid, A. H. M.; Auchus, R. J.; Hughes, B. A.; Cassidy, A. M.; Thompson, E.; Oommen, N. B.; Folkerd, E.; Dowsett, M.; Arlt, W.; de Bono, J. S. Clinical and Biochemical Consequences of CYP17A1 Inhibition with Abiraterone Given with and without Exogenous Glucocorticoids in Castrate Men with Advanced Prostate Cancer. *J. Clin. Endocrinol. Metab.* **2012**, *97*, 507−516.

(12) Malikova, J.; Brixius-Anderko, S.; Udhane, S. S.; Parween, S.; Dick, B.; Bernhardt, R.; Pandey, A. V. CYP17A1 Inhibitor Abiraterone, an Anti-Prostate Cancer Drug, Also Inhibits the 21-Hydroxylase Activity of CYP21A2. *J. Steroid Biochem. Mol. Biol.* **2017**, *174*, 192−200.

(13) Auchus, R. J.; Yu, M. K.; Nguyen, S.; Mundle, S. D. Use of Prednisone with Abiraterone Acetate in Metastatic Castration-resistant Prostate Cancer. *Oncologist* **2014**, *19*, 1231−1240.

(14) Petrunak, E. M.; DeVore, N. M.; Porubsky, P. R.; Scott, E. E. Structures of human Steroidogenic Cytochrome P450 17A1 with Substrates. *J. Biol. Chem.* **2014**, *289*, 32952−32964.

(15) Yadav, R.; Petrunak, E. M.; Estrada, D. F.; Scott, E. E. Structural Insights into the Function of Steroidogenic Cytochrome P450 17A1. *Mol. Cell. Endocrinol.* **2017**, *441*, 68−75.

(16) DeVore, N. M.; Scott, E. E. Structures of Cytochrome P450 17A1 with Prostate Cancer Drugs Abiraterone and TOK-001. *Nature* **2012**, *482*, 116−119.

(17) Potter, G. A.; Barrie, S. E.; Jarman, M.; Rowlands, M. G. Novel Steroidal Inhibitors of Human Cytochrome P45017.alpha.-Hydroxylase-C17,20-lyase): Potential Agents for the Treatment of Prostatic Cancer. *J. Med. Chem.* **1995**, *38*, 2463−2471.

(18) Garrido, M.; Peng, H. M.; Yoshimoto, F. K.; Upadhyay, S. K.; Bratoeff, E.; Auchus, R. J. A-ring Modified Steroidal Azoles Retaining Similar Potent and Slowly Reversible CYP17A1 Inhibition as Abiraterone. *J. Steroid Biochem. Mol. Biol.* **2014**, *143*, 1−10.

(19) Li, Z.; Bishop, A. C.; Alyamani, M.; Garcia, J. A.; Dreicer, R.; Bunch, D.; Liu, J.; Upadhyay, S. K.; Auchus, R. J.; Sharifi, N. Conversion of Airaterone to D4A Drives Anti-Tumour Activity in Prostate Cancer. *Nature* **2015**, *523*, 347.

(20) Pallan, P. S.; Wang, C.; Lei, L.; Yoshimoto, F. K.; Auchus, R. J.; Waterman, M. R.; Guengerich, F. P.; Egli, M. Human Cytochrome P450 21A2, the Major Steroid 21-Hydroxylase: Structure of the Enzyme/Progesterone Substrate Complex and Rate-Limiting C-H Bond Cleavage. *J. Biol. Chem.* **2015**, *290*, 13128−13143.

(21) Bonomo, S.; Hansen, C. H.; Petrunak, E. M.; Scott, E. E.; Styrishave, B.; Jorgensen, F. S.; Olsen, L. Promising Tools in Prostate Cancer Research: Selective Non-Steroidal Cytochrome P450 17A1 Inhibitors. *Sci. Rep.* **2016**, *6*, 29468.

(22) Trachtenberg, J.; Halpern, N.; Pont, A. Ketoconazole: A Novel and Rapid Treatment for Advanced Prostatic Cancer. *J. Urol.* **1983**, *130*, 152−153.

(23) Li, Z.; Alyamani, M.; Li, J.; Rogacki, K.; Abazeed, M.; Upadhyay, S. K.; Balk, S. P.; Taplin, M.-E.; Auchus, R. J.; Sharifi, N. Redirecting Abiraterone Metabolism to Fine-Tune Prostate Cancer Anti-Androgen Therapy. *Nature* **2016**, *533*, 547.

(24) Benoist, G. E.; Hendriks, R. J.; Mulders, P. F. A.; Gerritsen, W. R.; Somford, D. M.; Schalken, J. A.; van Oort, I. M.; Burger, D. M.; van Erp, N. P. Pharmacokinetic Aspects of the Two Novel Oral Drugs Used for Metastatic Castration-Resistant Prostate Cancer: Abiraterone Acetate and Enzalutamide. *Clin. Pharmacokinet.* **2016**, *55*, 1369−1380.

(25) Harris, R. K.; Becker, E. D.; Cabral de Menezes, S. M.; Goodfellow, R.; Granger, P. NMR Nomenclature: Nuclear Spin Properties and Conventions For Chemical Shifts. IUPAC Recommendations 2001. International Union of Pure and Applied Chemistry. Physical Chemistry Division. Commission on Molecular Structure and Spectroscopy. *Magn. Reson. Chem.* **2002**, *40*, 489−505.

(26) Madhra, M. K.; Sriram, H. M.; Inamdar, M.; Sharma, M. K.; Prasad, M.; Joseph, S. Improved Procedure for Preparation of Abiraterone Acetate. *Org. Process Res. Dev.* **2014**, *18*, 555−558.

(27) Bian, X.; Wang, L.; Liu, J.; Wang, C. Green Suzuki Coupling Reaction for Synthesis of Abiraterone Acetate and its Analogues. *J. Chem. Res.* **2016**, *40*, 289−292.

(28) Bu, M.; Cao, T.; Li, H.; Guo, M.; Yang, B. B.; Zeng, C.; Zhou, Y.; Zhang, N.; Hu, L. Synthesis And Biological Evaluation of Novel Steroidal 5α,8α-Epidioxyandrost-6-ene-3β-ol-17-(O-phenylacetamide)oxime Derivatives as Potential Anticancer Agents. *Bioorg. Med. Chem. Lett.* **2017**, *27*, 3856−3861.

(29) Chaubal, R.; Mujumdar, A. M.; Misar, A.; Deshpande, V. H.; Deshpande, N. R. Structure-activity Relationship Study of Androstene Steroids with Respect to Local Anti-inflammatory Activity. *Arzneim. Forsch.* **2006**, *56*, 394−398.

(30) Yu, J.; Zhou, Y.; Lin, Z.; Tong, R. Regioselective and Stereospecific Copper-Catalyzed Deoxygenation of Epoxides to Alkenes. *Org. Lett.* **2016**, *18*, 4734−4737.

(31) Bart, A. G.; Scott, E. E. Structural and Functional Effects of Cytochrome b5 Interactions with Human Cytochrome P450 Enzymes. *J. Biol. Chem.* **2017**, *292*, 20818−20833.

(32) Turcu, A. F.; Rege, J.; Chomic, R.; Liu, J.; Nishimoto, H. K.; Else, T.; Moraitis, A. G.; Palapattu, G. S.; Rainey, W. E.; Auchus, R. J. Profiles of 21-Carbon Steroids in 21-Hydroxylase Deficiency. *J. Clin. Endocrinol. Metab.* **2015**, *100*, 2283−2290.

(33) Motulsky, H. J.; Brown, R. E. Detecting Outliers When Fitting Data with Nonlinear Regression − A New Method Based on Robust Nonlinear Regression and The False Discovery Rate. *BMC Bioinf.* **2006**, *7*, 123.

(34) Kabsch, W. Xds. *Acta Crystallogr., Sect. D: Biol. Crystallogr.* **2010**, *66*, 125−132.

(35) Collaborative Computational Project, N.. The CCP4 Suite: Programs for Protein Crystallography. *Acta Crystallogr., Sect. D: Biol. Crystallogr.* **1994**, *50*, 760−763.

(36) McCoy, A. J.; Grosse-Kunstleve, R. W.; Adams, P. D.; Winn, M. D.; Storoni, L. C.; Read, R. J. Phaser Crystallographic Software. *J. Appl. Crystallogr.* **2007**, *40*, 658−674.

(37) Adams, P. D.; Afonine, P. V.; Bunkoczi, G.; Chen, V. B.; Davis, I. W.; Echols, N.; Headd, J. J.; Hung, L. W.; Kapral, G. J.; Grosse-Kunstleve, R. W.; McCoy, A. J.; Moriarty, N. W.; Oeffner, R.; Read, R. J.; Richardson, D. C.; Richardson, J. S.; Terwilliger, T. C.; Zwart, P. H. PHENIX: A Comprehensive Python-based System for Macromolecular Structure Solution. *Acta Crystallogr., Sect. D: Biol. Crystallogr.* **2010**, *66*, 213−221.
(38) Emsley, P.; Lohkamp, B.; Scott, W. G.; Cowtan, K. Features and Development of Coot. *Acta Crystallogr., Sect. D: Biol. Crystallogr.* **2010**, *66*, 486−501.
(39) *The AxPyMOL Molecular Graphics Plugin for Microsoft PowerPoint*, 1.0; Schrodinger, LLC, 2010.
(40) Friesner, R. A.; Banks, J. L.; Murphy, R. B.; Halgren, T. A.; Klicic, J. J.; Mainz, D. T.; Repasky, M. P.; Knoll, E. H.; Shelley, M.; Perry, J. K.; Shaw, D. E.; Francis, P.; Shenkin, P. S. Glide: A New Approach For Rapid, Accurate Docking and Scoring. 1. Method and Assessment of Docking Accuracy. *J. Med. Chem.* **2004**, *47*, 1739−1749.
(41) Li, J.; Abel, R.; Zhu, K.; Cao, Y.; Zhao, S.; Friesner, R. A. The VSGB 2.0 Model: A Next Generation Energy Model for High Resolution Protein Structure Modeling. *Proteins: Struct., Funct., Genet.* **2011**, *79*, 2794−2812.